UNIVERSITY OF CALIFORNIA SAN DIEGO

Tracking Ontogenetic Changes of Ionocyte Distribution and Morphology in Larval White Seabass (*Atractoscion nobilis*)

A Thesis submitted in partial satisfaction of the

requirements for the degree

Master of Science

in

Marine Biology

by

Shane Harrison Finnerty

Committee in Charge:

Professor Martin Tresguerres, Chair
Professor Ronald Burton
Professor Phil Hastings

2019

The Thesis of Shane Harrison Finnerty is approved, and it is acceptable in quality and form for publication on microfilm and electronically:

_____

_____

_____
Chair

University of California San Diego

2019

DEDICATION

I would like to dedicate this thesis to my family, friends, colleagues, and mentors who have contributed love, positivity, guidance, and inspiration in my life. Of the many who have participated, there are a few who I would like to give special recognition.

My father Harry and mother Carolina, who instilled in me pride, self-love, and an understanding that personal growth is forged through hard work and determination. My brothers Noah and Geoff, who have always been there in friendship and laughter. To my Uncle Bob, Aunt Barb and Cousin Wilson, for tossing me into the crashing waves of Asilomar, of which I largely attribute towards my love of the ocean.

To my many friends: Ryan Waldman, David Aufai, Rachel Ryba, Tyson Shroyer, Kiya Driscoll Michelina D'Amore, and the entirety of the Creepy Crew! To Alec Althuisius, one of my dearest friends, who's impact on my life will never be forgotten. May he rest in peace. You all have shown me the true meaning of love and friendship, and the importance of living life for everything it can be.

To Michelle Paddack, for opening my eyes to wonders of marine biology, and for being a true inspiration as an ocean advocate.

To the Tresguerres Lab. I could not have made it through the countless hours of lab work and writing without all of your support, encouragement, cold beers, and comedic relief.

Thank you to each and every one of you who has contributed in making the creation of this Thesis possible, and supporting me in attaining the greatest achievement of my life.

EPIGRAPH

"The true biologist deals with life, with teeming boisterous life, and learns something from it, learns that the first rule of life is living."
-John Steinbeck

"Look up at the stars and not down at your feet. Try to make sense of what you see, and wonder about what makes the universe exist. Be curious."
-Stephen Hawking

"They both listened silently to the water, which to them was not just water, but the voice of life, the voice of Being, the voice of perpetual Becoming."
-Herman Hesse

"The sea, once it casts its spell, holds one in its net of wonder forever"
-Jacques Yves Cousteau

"[*Referring to the shark that ate his friend, Esteban*] I'll fight it, but I won't kill it. Now, what about my dynamite?"
-Steve Zissou

TABLE OF CONTENTS

Signature Page iii

Dedication iv

Epigraph v

Table of Contents vi

List of Abbreviations vii

List of Figures ix

Acknowledgements xi

Abstract of the Thesis xiii

Introduction 1

Materials & Methods 11

Results 18

Discussion 32

References 40

LIST OF ABBREVIATIONS

BL	Body length
Ca^{2+}	Calcium
Cl^-	Chloride
CLSM	Confocal laser scanning microscopy
DIC	Differential interference contrast
DPH	Days post hatch
HSWRI	Hubbs SeaWorld Research Institute
K^+	Potassium
LPM	Liters Per Minutes
Na^+	Sodium
NaCl	Sodium chloride
NH_3	Ammonia
NH_4^+	Ammonium
NHE	Sodium-Hydrogen Exchanger (Na^+/H^+ Exchanger)
NKA	Sodium-Potassium ATP-ase (Na^+/K^+ ATP-ase)
OREHP	Ocean Resources Education and Hatchery Program
PBS	Phosphate buffered saline
PVDF	Polyvinylidene difluoride
RIA	Relative ionocyte Area
RTU	Ready to use
SA/Vol	Surface area to volume
SEM	Scanning electron microscopy

tBa	Tert-butyl alcohol
TBS-T	Tris-buffered saline + 1% tween

LIST OF FIGURES

Figure 1: A) From Evans et al., 2005. Transmission electron micrograph of an ionocyte from the gills of a marine teleost. Note the size of the apical crypt (pit) in comparison to the highly infolded basolateral membrane. B) From McCormick 2012. Mechanism of NaCl excretion in a marine teleost ionocyte 6

Figure 2: From Kwan et al. 2018. Cutaneous ionocytes from yellowfin tuna larvae. A) Ionocytes with widened apical surfaces and extended microvilli. B) Ionocytes with reduced apical surfaces and retracted microvilli 6

Figure 3: Change in body length in relation to age throughout larval White Seabass development 19

Figure 4: Western blot with anti-NKA monoclonal antibodies. *CH* crude homogenate, *CY* cytosolic fraction, *MB* membrane fraction. 19

Figure 5: Na^+/K^+ immunostained light microscopy images showing four developmental stages of White Seabass larvae. A) Pre-flexion larvae, 3.49 mm BL (3 DPH). B) Flexion larvae, 6.33 mm BL (15 DPH). C) Post-flexion larvae, 7.83 mm BL (21 DPH). D) Transformation larvae, 11.1 mm BL (31 DPH). 20

Figure 6: Na^+/K^+ immunostained light microscopy images of development of gill structures and presence of ionocytes in a developmental series of White Seabass larva 21

Figure 7: A) Number of cutaneous ionocytes in larval White Seabass ranging from 2.6 mm to 16.4 mm BL. B) Inlay of dotted box in graph 2A 23

Figure 8: Change in ionocyte size in the A) head, B) trunk, and C) fins in larval White Seabass ranging from 2.6 mm to 16.4 mm BL 24

Figure 9: Cutaneous ionocyte area relative to total skin surface area in larval White Seabass ranging from 2.6 mm to 16.4 mm BL in relation to A) days post-hatch and B) body length 25

Figure 10: Change in ionocyte size in the A) head, B) trunk, and C) fins in larval White Seabass ranging from 2.6 mm to 16.4 mm BL 27

Figure 11: Differences in ionocyte size between head, trunk, and fin regions of White Seabass larvae in 3-5 mm BL, 6-8 mm BL, 9-11 mm BL, and 12-15 mm BL size groups. Grey circles denote average size of head ionocytes, black squares denote average size of trunk ionocytes, dark grey triangles denote average size fin ionocytes 28

Figure 12: SEM images of various ionocyte morphologies in the gill versus skin of a 32DPH White Seabass larva 29

Figure 13: Three-dimensional rendering of an ionocyte on the skin of a juvenile White Seabass. (A) DIC view of the apical morphology of pavement cells and an ionocyte. (B) lateral view of the ionocyte. (C) DIC view 5μm below the depth at which (A) was captured. (D) lateral view of (C). (E) and (F) lateral view at higher magnification 31

ACKNOWLEDGEMENTS

I would like to acknowledge and thank several key figures who scientific knowledge, skill, and mentorship played pivotal roles in the creation of this thesis.

Martin Tresguerres, principle investigator and the chair of my thesis committee, provided sound advice, encouragement to always strive in producing better work, and was always present and participatory from the very beginning. I must also note he cooks some of the best barbeque I have ever had the pleasure of eating.

Garfield Kwan, my mentor and friend, invested countless hours of his time equipping me with the knowledge and lab skills that allowed me to succeed as a graduate student. I learned a great deal not only from Garfield's laboratory work and writing ability, but also from his endless determination to produce quality science, and a passionate will to help others succeed.

Nick Wegner, for the opportunity to volunteer on several projects at NOAA's South West Fisheries Science Center and for teaching me how to prepare fish larvae for use in scanning electron microscopy.

Phil Zerofski, for helping me to pursue my interests in field work, and the many opportunities to aid in specimen collections, and exploration of Scripps Canyon and the surrounding kelp forests which I love so much.

I would also like to acknowledge Ronald Burton and Phil Hastings for participating as members of my thesis committee. I learned a great deal in the courses they taught during my undergraduate and graduate career, and am incredibly grateful for the time and knowledge they have invested in me during the creation of this thesis.

The work in this thesis would not be possible without the generous contribution of time and effort from the team at Hubbs SeaWorld Research Institute. I would especially like to thank

Erica Brombay-Fanning who was the primary care taker of the larvae used in this study, and Mark Drawbridge, the senior researcher of HSWRI's aquaculture research project.

Funding for this study was provided by the National Science Foundation, IOS #1754994.

ABSTRACT OF THE THESIS

Tracking Ontogenetic Changes of Ionocyte Distribution and Morphology in Larval White Seabass (*Atractoscion nobilis*)

by

Shane Harrison Finnerty

Master of Science in Marine Biology

University of California San Diego, 2019

Professor Martin Tresguerres, Chair

Teleost fishes maintain homeostasis through the action of ionocytes, epithelial cells specialized for osmoregulation, acid-base regulation, and ammonia excretion, among other functions. While studied extensively in adult fishes, much less is known about ionocytes and their function in marine teleost larvae. The goal of this thesis is to track the ontogenetic changes in number, size, distribution, and morphology of ionocytes in skin and gills of larval White Seabass (*Atractoscion nobilis*) ranging from 1-32 days post-hatch (2.6 to 16.4 mm body length). Immunostaining of ionocytes revealed a stark increase in ionocyte number and density, and a

decrease in ionocyte size throughout the sample period. Relative ionocyte area, a proxy for ion excretion across the skin, was calculated revealing a decrease in cutaneous ion excretion prior to the timing of notochord flexion. During this period, the branchial structures became increasingly developed and were highly abundant in ionocytes, suggesting they are taking on a large portion of the ionoregulatory role. Scanning electron microscopy revealed several different apical morphologies in a 32 DPH larva, and confocal scanning laser microscopy revealed the presence of ionocyte in the skin of a juvenile White Seabass. This is the first study to provide high temporal resolution tracking of the ontogenetic changes of ionocytes in larval White Seabass, who were selected due to their high socio-economic value and for the increasing demand for research to aid in the wild stock enhancement aquaculture program operated by Hubbs SeaWorld Research Institute (San Diego).

INTRODUCTION

The ability of an organism to maintain homeostasis despite changes in the external environment is crucial to all life on Earth. Whether it be maintaining a stable internal temperature, pH, osmolarity or ion concentration, the ability to regulate internal physiological conditions has allowed life to expand into the multitude of environments where it is found today. Marine bony fishes (teleosts) are one of the most successful and diverse lineages of organisms on the planet, a characteristic that can be attributed in part to their impressive ability maintain osmotic homeostasis despite living in aquatic environments with salinities three to four times that of their internal fluids. While these mechanisms have been studied extensively in adult teleosts, much less information exists about the osmoregulatory capabilities of teleost larvae, and even less so concerning the osmoregulatory capabilities of marine teleost larvae. This is at least partially due to the difficulties associated with raising marine teleost larvae from embryo throughout larval stages in a laboratory setting, which is much more difficult compared to some freshwater species such as zebrafish and trout. As a result, the physiology and developmental biology of marine teleost larvae remains an exciting and relatively unexplored field of science. White Seabass (*Atractoscion nobilis*) were chosen as the experimental species in my thesis for their high socio-economic value and for the increasing demand for research to aid in the wild stock enhancement aquaculture program operated by the Hubbs SeaWorld Research Institute, located nearby to Scripps Institution of Oceanography (San Diego, CA) where this study was conducted.

White Seabass

White Seabass are the largest member of the Sciaenidae, or croaker, family found along the coast of the north-eastern Pacific Ocean. They inhabit areas over the continental shelf from

Juneau, Alaska, to Magdalena Bay, Baja California, as well as within the northern Gulf of California (Moser et al., 1983; Thomas 1968). Often referred to as "ghosts" by the recreational fishing community, White Seabass in the wild are illusive due to the wide variety of habitats they live and forage in. During their typical mating season, from April through August, they can be found in schools over rocky reef structures, sandy shores, or within kelp forests (Thomas, 1968). During colder months, White Seabass typically remain in deeper waters, around 30m depth, until water temperatures begin to warm in spring and summer when they will return to shallower waters to spawn. They are considered a highly mobile coastal species, in that some tagged individuals have been observed moving over 500km within a 3-month period (Aalbers & Sepulveda, 2015). Fisheries and mark-recapture data have shown that White Seabass tend to return to specific areas from year to year, most likely in search of prey. They display a strictly carnivorous diet, feeding primarily on small pelagic fishes such as sardine, mackerel, anchovy, herring, as well as squid and pelagic crabs (Vojkovich & Reed, 1983). Their active lifestyle and protein-rich diets allow them to reach averages of around 60 pounds in adulthood, but the current California record stands at 93 pounds, taken by speargun off of Laguna Beach in 2007 (Thomas 1968, "White Seabass").

Because of their large size and high-quality meat, White Seabass have been a highly targeted species by both commercial and recreational fisheries along the north eastern Pacific since the early 1900's, with efforts primarily focused around Santa Catalina and San Clemente islands. In 1920, annual commercial catches reached upwards of 2.5 million pounds, primarily through the use of purse seining (Thomas, 1968). From the early 1950s to the 1980s however, the White Seabass fishery, one of California's most historic and economically successful fisheries, began to collapse. By 1981, the commercial catch had dropped to roughly 10% of their

typical historic catch abundance (Allen et al., 2007; Vojkovich & Reed, 1983). Coastal development likely contributed to the decline of the White Seabass population as well. High abundances of larvae and juveniles have been observed in coastal bays, estuaries, and shallow sandy embayments along the coast of the Southern California Bight and the western coast of Baja California, Mexico (Allen & Franklin, 1991; Moser et al., 1983). With a large majority of Southern California's coastal wetland habitat being lost to development within the last several decades, large estuarine environments which once acted as suitable habitats for larval settlement and growth, are now gone. A combination of overfishing and loss of coastal habitat led to a collapse of the White Seabass fishery by the end of 1982.

In response to the collapse of the fishery, California legislation established the Ocean Resources Education and Hatchery Program (OREHP) to aid in restocking wild populations of marine fish caught in Southern California. Initially the program focused both on White Seabass and California Halibut (*Paralichthys californicus*), but eventually shifted the bulk of its focus to White Seabass due to budget constraints and a severe depression of wild stock. In 1995, OREHP funded the construction of a White Seabass hatchery in Carlsbad, California which is owned and operated by Hubbs-SeaWorld Research Institute (HSWRI). The 22,000 square foot hatchery facility is capable of producing more than 350,000 juvenile White Seabass annually, who are raised from hatch to roughly 150-200 mm standard length. They are then electronically tagged and moved to one of 14 satellite grow out facilities scattered throughout the Southern California Bight, including one facility on Santa Catalina Island. When the juvenile fish reach roughly 300 mm standard length, they are released from their grow-out pens to join the wild White Seabass stocks (CalCOFI 2006, "Ocean Resources Enhancement and Hatchery Program", "Hubbs SeaWorld Research Institute Facilities").

HSWRI's hatchery presents a valuable opportunity to study the biology and physiology of White Seabass, and to improve aquaculture techniques in general. The hatchery maintains a broodstock of wild-caught adult White Seabass who's spawning behavior can be regulated by modifying the photoperiod and temperature of the water. Once the broodstock fish spawn, the eggs are collected and set to hatch in separate grow-out tanks for production or experimental purposes. The water chemistry in the broodstock tanks are closely regulated and recorded daily in logs dating back to the establishment of the hatchery. This long-standing data set, in addition to the ability to successfully raise large quantities of healthy White Seabass, make HSWRI a valuable asset in better understanding the early development of White Seabass, and marine teleosts in general.

Osmoregulation is Mediated by Ionocytes in Marine Teleosts

Osmoregulation is the ability of an organism to actively regulate internal fluid osmolarity through control of water and ion concentrations. Marine teleosts maintain an internal fluid osmolarity between ~300-400mOsm, and Na^+ and Cl^- concentrations both around ~175mM. Seawater has an osmolarity of ~1,000mOsm, and Na^+ and Cl^- concentrations of ~450mM (Evans, 2005). This steep osmotic and ionic gradient causes water to flow out of the fish by osmosis and NaCl to enter the bloodstream by diffusion. If unregulated, dehydration and ion imbalance within the internal fluids of the fish would adversely affect physiological performance and eventually lead to death. However, marine teleosts have evolved osmoregulatory mechanisms whereby they obtain H_2O through ingestion of seawater and excrete excess NaCl through specialized cells known as ionocytes.

Ionocytes are epithelial cells that are specialized for transporting ions between the bloodstream and the surrounding water through the action of multiple transport proteins localized

in the apical and basolateral membranes of the cell. First described as “chloride-secreting cells” by Keys & Willmer (1932), the term ionocyte (also referred to as “mitochondria rich cell”) is now preferred after discovery of several other cellular functions including Na^+, Cl^-, and other ions secretion and absorption, acid/base regulation, and ammonia excretion (Hiroi & McCormick, 2012; Rombough, 1999). The driving force for NaCl secretion by ionocytes is provided by the enzyme Na^+/K^+-ATPase (NKA), which is abundant in the basolateral membrane. NKA uses the energy from ATP hydrolysis to transport three sodium (Na^+) from the cell into the bloodstream in exchange for two potassium (K^+). This lowers the intracellular [Na^+] and drives the secondary active transport of Na^+ and Cl^- out of the bloodstream through para-cellular and trans-cellular pathways, respectively. Ionocytes in marine teleosts are capable of excreting NaCl against steep electrochemical gradients due to the incredible abundance of NKA within the highly infolded basolateral membrane of the cell. The membrane forms a complex tubular system with extremely high surface area extending throughout the cytoplasm and is closely associated with mitochondria that supply NKA with energy in the form of ATP. The apical membrane is relatively small in surface area compared to the basolateral membrane and forms a concave apical “pit”. The morphology of the apical membrane has been observed in several forms. Varsamos et al. (2002) showed that branchial (gill) ionocytes of the marine European Sea Bass (*Dicentrarchus labrax*) exhibited widened apical surfaces and extended microvilli in response to increasing salinities. Kwan et al. (2018) showed that cutaneous ionocyte apical membrane area decreased, and microvilli became reduced, throughout larval development in Yellowfin Tuna (*Thunnus albacarus*). These data suggest that the apical morphology of ionocytes can dynamically change, possibly as a regulatory mechanism for diverse physiological functions; however the actual significance remains unclear.

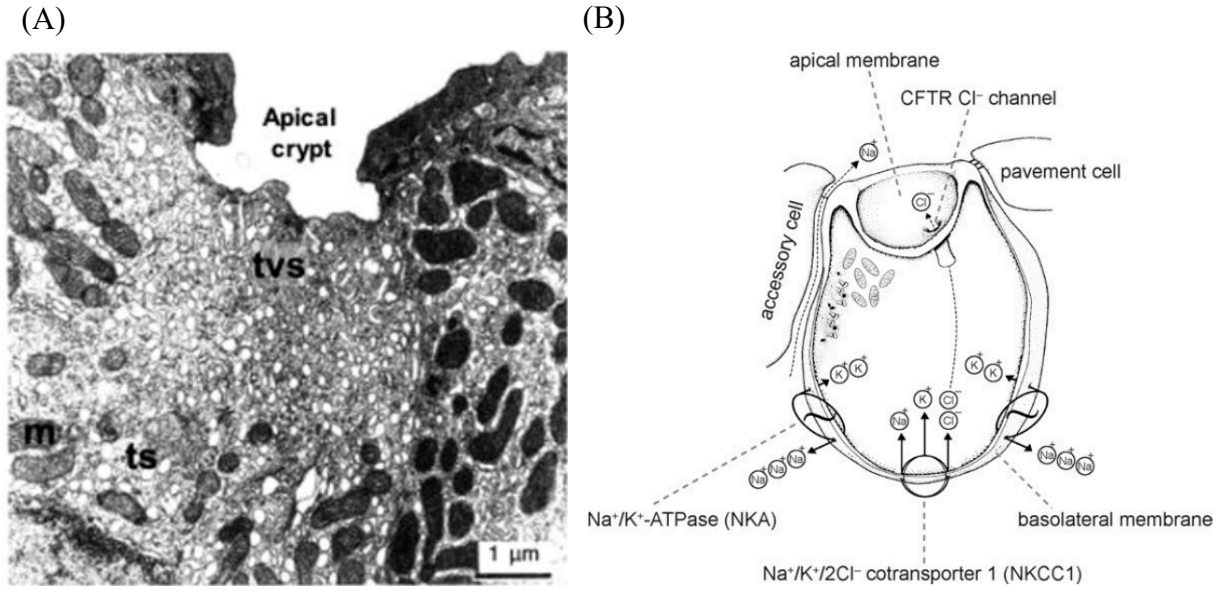

Figure 1: A) From Evans et al., 2005. Transmission electron micrograph of an ionocyte from the gills of a marine teleost. Note the size of the apical crypt (pit) in comparison to the highly infolded basolateral membrane. (m) mitochondria, (ts) tubular system, (tvs) subapical tubulovascular system. B) From McCormick 2012. Mechanism of NaCl excretion in a marine teleost ioncoyte. The apical membrane and basolateral membranes are in contact with seawater and the bloodstream, respectively. Basolateral NKA hydrolyses ATP to drive secretion of NaCl through the secondary active transport proteins NKCC, in the basolateral membrane, and CFTR, in the apical membrane. Not shown is the abundant infoldings of the basolateral membrane.

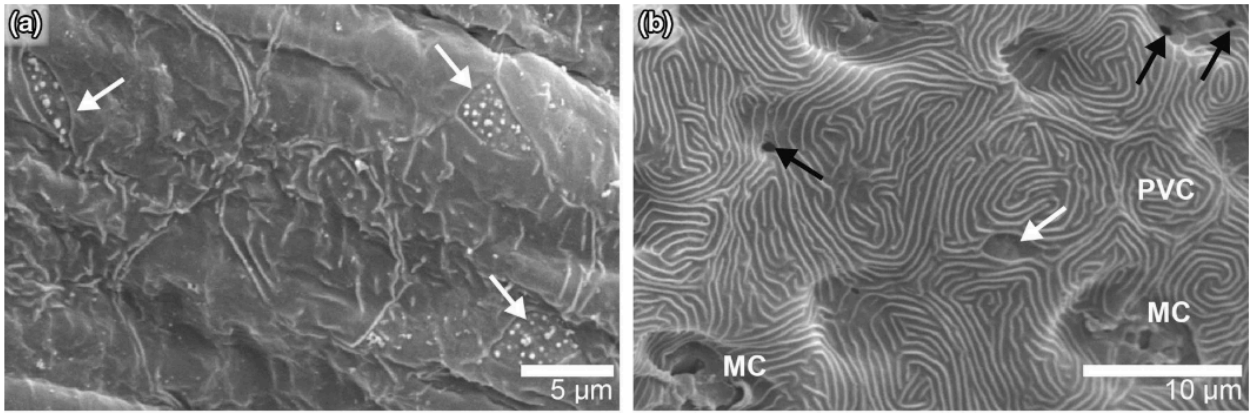

Figure 2: From Kwan et al. 2018. Cutaneous ionocytes from yellowfin tuna larvae. A) Ionocytes with widened apical surface and extended microvilli in a 3.8 mm BL (10 days post-hatch) larvae. B) Ionocytes with reduced apical surface and retracted microvilli in a 6.5 mm BL (16 days post-hatch).

Additional Ion Transport Functions of Ionocytes

In addition to excretion of NaCl, ionocytes have been shown to be involved in several other transport mechanisms including acid-base regulation, ammonium excretion, and calcium (Ca^{2+}) uptake. Na^+/H^+ exchangers (NHEs) in the apical membrane of both freshwater and marine

teleost ionocytes mediate H^+ secretion in exchange for Na^+ in a secondarily active transport mechanism driven by basolateral NKA (reviewed in Evans, 2005 and Hwang, 2011). In freshwater and seawater adapted larval Medaka (*Oryzias latipes*) [Liu et al., 2013] and adult Climbing Perch (*Anabas testudines*) [Chen et al. 2017], ammonia gas (NH_3) is excreted from blood to the water by diffusion as well as by facilitated transport *via* apical Rheusus glycoproteins located in the apical membrane of ionocytes. Recent data suggests NHEs are also involved this ammonia excretion mechanism by creating an acidic boundary layer that pronates NH_3 thus trapping it outside of the apical membrane in the form of NH_4 (Wu et al., 2010). However, it is not known if this mechanism is found in other marine teleosts. Ionocytes also play an essential role in Ca^{2+} uptake in freshwater teleosts living in soft-water environments (i.e. with little dissolved Ca^{2+}) (Flik et al., 1995; Marshall et al., 1992). This mechanism relies on apical Ca^{2+} channels and the basolateral ion transporters: Plasma membrane Ca^{2+}-ATPase 2 (PMCA2), Na^+/Ca^{2+} exchanger 1b (NCX1b), and NKA to transport Ca^{2+} from the surrounding water into the bloodstream (Lin & Hwang, 2016). However, seawater has much greater dissolved $[Ca^{2+}]$ compared to fish blood, so it is not clear whether marine teleosts require similar ionocyte Ca^{2+} uptake mechanisms.

Developmental Stages of Teleost Larvae

Teleost larval metamorphosis can be separated into several developmental stages, each defined by key morphological changes. In this study, metamorphosis was divided into four stages: pre-flexion, flexion, post-flexion, and transformation. Pre-flexion begins at hatch and ends at the start of notochord flexion and marks the time of yolk-sac absorption and formation of the eyes, mouth, and gut. Flexion begins with the dorsal bending of the notochord tip and is co-current with separation of the median finfold and beginning of fin-ray formation. Post-flexion

begins once the dorsal tip of the notochord has reached a ~45° angle and ends at the beginning of transformation, the final stage in larval development before reaching the juvenile stage. Transformation larvae possess features characteristic of early juvenile fish including complete separation of dorsal, caudal, and anal fins, well developed fin spines and rays and a well-developed jaw structure.

Teleost Gill Development and Ontogeny of Ionocyte Distribution

Teleosts have four pairs of gills, each composed by an arch, filaments, and lamellae. Two rows of filaments extend vertically outward from each arch, and a row of lamellae extend horizontally out from both sides of each filament. This structure provides a high surface area of a thin epithelium that is ideal for both gas and ion exchange. Generally, gill arches form by the time of hatch or shortly after, followed by development of filaments and then lamellae. The development of the branchial structures is believed to correspond to an increasing demand for ion and gas exchange area as the larvae increase in size. Timing of each step in this developmental series varies both interspecifically and in response to environmental conditions; Factors such as temperature, salinity and dissolved oxygen concentration have large impacts on larval development, and likely effect the timing of gill structure formation. In the Turbot, (*Scophthalmus maxius*) acclimated to brackish water and kept between 16 and 20°C, gill arches are present at 4 days post-hatch (DPH) followed by filament formation at 10 DPH (Segner et al., 1994), whereas in freshwater acclimated Rainbow Trout (*Onchorhynus mykiss*) kept at 10°C, gill arches and filaments are present 6 and 3 days before hatch, respectively (Rombough, 1999). Increased growth and survival rates have been observed in response to decreased salinities in larval marine Mulloway (*Argyrosomus japonicus*) [Fielder & Bardsley, 1999], Southern Flounder (*Paralichthys lethostigma*) [Smith et al. 1999], and Gilthead Seabream (*Sparus aurata*)

[Tandler et al. 1995] and increased pO_2 in larval Yellowfin Tuna (Wexler et al., 2011). However, little attention has been focused on the effects these conditions have on gill formation specifically.

At hatch, ionocytes are exclusively present on the skin of the larva. However, gill ionocytes eventually appear and continuously increase in number throughout larval development. It is generally believed that the gills accumulate a higher number of ionocytes than the skin by the end of larval metamorphosis. While the functional transition of ionocytes from skin to gills follows a similar pattern in all species, large differences exists regarding the timing and rate of transition across different species and rearing conditions (Rombough, 1999; Varsamos, 2005). For example, ionocytes appeared on developing gill filaments of the Japanese Flounder (*Paralichthyes olivaceus*) [Hiroi et al., 1998] and the Yellowfin Tuna (*Thunnus albacares*) [Kwan et al., 2018] during pre-flexion, and their number continuously increased throughout larval development in both species. However, while in flounder the number of cutaneous ionocytes progressively decreased following notochord flexion and completely disappeared by the end of metamorphosis, in yellowfin tuna they continuously increased throughout metamorphosis.

This is just one example of interspecific differences that exist concerning changes in ionocyte localization and abundance in the skin and gills of teleost larvae throughout metamorphosis. (more examples are reviewed in Varsamos, 2005). Such differences, if more thoroughly studied, can lend insight to the developmental biology and life history of different teleost species. Larval metamorphosis is a period of both increased mortality and rapid development of key morphological features in teleosts. Species-specific differences concerning

ionocytes during this life stage may be related to the vulnerability or resilience of certain species, and is worthy of further exploration.

Thesis goals

The goals of this study are to characterize changes in cutaneous ionocyte size, density, distribution and morphology in larval White Seabass throughout early development, and to speculate on potential roles of cutaneous ionocytes besides NaCl excretion. Access to a comprehensive developmental series of larvae from Hubbs SeaWorld Research Institute's White Seabass hatchery, together with immunohistochemistry and imaging techniques allowed for high accuracy quantification and tracking of cutaneous ionocytes throughout larval metamorphosis. This study is the first to describe the functional transition of ionocytes from the skin to the gills in larval White Seabass and can serve as a baseline study for use in developmental biology, comparative physiology, and aquaculture research.

MATERIALS & METHODS

Larval rearing conditions

A developmental series of White Seabass ranging from 2.6–16.4 mm body length (BL) corresponding to 1-32 days post hatch were collected from a standing broodstock of adult White Seabass raised and maintained at Hubbs SeaWorld Research Institute's hatchery facility located in Carlsbad, California. The broodstock fish spawn on a fixed schedule which is regulated by alteration of the temperature and photoperiod to mimic natural spring-summer conditions. Fish typically reach peak spawning behavior when water temperatures reach 17-18ºC. Fertilized eggs are collected with a 500 µm mesh net mounted on the outflow of the broodstock tank then transferred to larval rearing tanks to hatch. The tanks run on an open-flow through water system which receives filtered and UV sterilized seawater (34 ‰) pumped into the facility from Agua Hedionda Lagoon located just outside the hatchery.

The larvae were maintained in 320-liter cylindrical tanks with a flow rate beginning with 1 liter per minute (LPM) at hatch which was slowly raised to 6 LPM by the end of the sample period. Larval tanks were kept on an 18-hour light, 6-hour dark cycle throughout the sample period. Larvae were fed 1st instar artemia starting at a rate of 3/ml at 4 DPH, were weaned onto enriched 2nd instar artemia between 6-8 DPH, and ate 2nd instar artemia until being weaned onto dry food between 21-29 DPH. Water temperature in the larval tanks was kept between 19.0-19.6°C, dissolved oxygen between 8.79-9.29 mg/L, and pH between 7.86-8.31. Each day 10-20 larvae were collected, anesthetized with MS-222 and fixed in 4% paraformaldehyde for 6-8 hours, transferred to 70% ethanol, and stored at 4ºC until being processed for ionocyte immunolabeling. Additional larvae were collected at a later date from a separate spawning event, as unbeknownst to us 4% paraformaldehyde is not an effective fixative for scanning electron

microscopy (SEM). These larvae were raised under similar conditions as the first set, but instead were fixed in a 3% paraformaldehyde, 0.35% glutaraldehyde, 0.1M cacodylate buffer fixative (cat # 15949 Electron Microscopy Sciences, Hatfield, PA, USA) until being processed for SEM.

Western Blot Analysis

The specificity of the anti NKA α5 monoclonal antibody used for whole mount immunohistochemistry in this study has been validated in several elasmobranch and teleost species (Kwan et al. 2018; Roa et al. 2014; Roa & Tresguerres, 2017). Western blot analysis was conducted to verify its specificity in White Seabass larvae used in this study. Three 32 DPH larvae were anesthesized in MS-222, immediately frozen using dry ice, and stored at -80°C until processing. Frozen larvae were pulverized using mortar and pestle and mixed in an ice-cold protease inhibiting buffer. Samples were then spun down and separated into crude homogenate, cytosolic and membrane fractions. Total protein concentrations were determined using Bradford Assay, and 5 μg of protein combined with 2x Laemmli buffer and 2-beta mercaptoethanol were loaded into each lane after heating at 70°C for 5 minutes. Proteins were separated in a pre-cast polyacrylamide gel (cat # 4568124, Bio-Rad Laboratories, Hercules, CA, USA) at 200V for 50 minutes. Proteins were then transferred to a polyvinylidene difluoride (PVDF) membrane using a wet transfer cell immersed in Towbin's buffer at 100mA overnight (Bio-Rad). After transfer the PVDF membrane was incubated in blocking buffer at room temperature for 1 hour then incubated in the anti NKA α5 monoclonal antibody (10.5 ng/mL) at 4°C overnight. The following morning, the PVDF membrane was washed three times in Tris-buffered saline +1% tween (TBS-T), incubated in goat anti-mouse HRP-linked secondary antibodies (21ng/mL) at room temperature for 1 hour, and washed three times in TBS-T. Clarity Western ECL Substrate

(Bio-Rad) was used to reveal protein bands, followed by imaging and analysis in a Bio-Rad Universal III Hood with ImageQuant software (Bio-Rad).

Immunolabeling of ionocytes

Ionocytes in the skin and gills were immunolabeled using immunohistochemistry techniques described in Kwan et al (2018, 2019). A Vector-Stain Ready-to-Use (RTU) kit was used in conjunction with a DAB Peroxidase (3, 3' -diaminobenzidine) (Vector Laboratories, Burlingame, USA) to locate ionocytes on the skin of whole White Seabass larvae. Fixed samples were washed in tap water for 10 minutes followed by a 1-hour wash in 3% H_2O_2 to reduce pigmentation and background staining. Samples were then incubated in normal horse serum found in the Vector RTU kit for 20 minutes, and then incubated with an α5 mouse monoclonal antibody raised against the α-subunit of chicken NKA in blocking buffer (21ng/mL). The following day the samples were washed in phosphate buffered saline (PBS) for 5 minutes 3 times, followed by a 45-minute wash with a pan-specific secondary antibody from the Vector RTU kit. Another 3x5 minute PBS wash was then administered followed by a 15-minute streptavidin peroxidase wash. Following a third 3x5 PBS wash, the samples were incubated in DAB stain for 30 seconds, then rinsed in deionized water before imaging. A subset of samples was incubated overnight in blocking buffer without any primary antibodies as negative controls and had no specific staining. Samples were kept in a 0.02% sodium azide solution for long-term storage.

In addition to the larvae from HSWRI that were stained using DAB-peroxidase as described above, a small section of skin from a ~6-month old White Seabass hatched at HSWRI and raised in an experimental aquarium at Scripps Institution of Oceanography was immunolabelled using fluorescent secondary antibodies for imaging with confocal laser scanning

microscopy (CLSM). A modified version of the DAB staining protocol was used, wherein goat anti-mouse Alexa Fluor 546 secondary antibodies (4µg/mL) were used instead of the pan-specific secondary antibodies included in the Vector RTU kit, and the DAB staining step at the end of the protocol was skipped. This sample was imaged separately using a Zeiss Axio Observer LSM800 confocal laser scanning microscope.

Whole Mount Larval Imaging

Smaller White Seabass larvae (< ~6.5 mm BL) were imaged using a Leica S8APO compound microscope and larger larvae (> ~6.5 mm BL) were imaged using a Leica MZ9.5 stereomicroscope (Lecia Microsystems Inc.). Both microscopes were mounted with Canon Rebel T3i single reflex cameras and image capture was controlled using a Canon RC-6 wireless remote. In order to obtain images with three-dimensional resolution, a series of images was obtained at progressive focal planes through the right side of the larvae and then z-stacked using Helicon Focus software (HeliconSoft Ltd.). Because the larvae were much larger than the cameras viewing angle, many focal series had to be collected and z-stacked, then stitched together using Adobe Photoshop CS6 (Adobe Inc., San Jose, CA), resulting in high resolution images that covered the entire surface of the right side of each larvae which were used for subsequent cutaneous ionocyte quantification (This process is described in greater detail in Kwan et al. 2019). In addition, the left operculum was removed, and branchial structures were extracted for imaging at incremental time points throughout the sample period. Micro-dissecting probes were constructed for extracting branchial structures from smaller larvae (<5 mm BL), as standard probes were too large to dissect the minute structures. Micro-dissecting probes were constructed by first pulling the tip of a glass pipette using forceps and a Bunsen burner, then inserting the warm tip into bee's wax. While the wax was still warm in the tip, a micro-dissecting needle was

carefully inserted into the wax. The micro-dissecting needle was of a small enough diameter, that the operculum and branchial structures of very small larvae could be removed with minimal damage. Isolated gills were then carefully mounted onto glass microscope slides for imaging. The right pectoral fin was also removed from each larva as it obstructed the view of cutaneous ionocytes beneath it, and the number of cutaneous ionocytes on the pectorals was negligible in comparison to the total number of cutaneous ionocytes (<6%; 11.13 mm BL larva: 786 pectoral ionocytes out of 14,089 total ionocytes; 16.402 mm BL larva: 898 pectoral ionocytes out of 36,516 total ionocytes).

Quantification Techniques

Digital images were used to measure larval body length and total area, and to count or estimate cutaneous ionocyte number and average size using Fiji image analysis software (version 1.0). Body length was measured as the distance from the anterior tip of the snout to the posterior tip of the notochord using the straight-line tool. Total area was measured as the total surface area of the right side of the larvae using the freehand tool. Ionocytes were identified by their dark coloration resulting from the intense NKA immunostaining. Using the cell counter tool, all ionocytes on the right side of each larvae < 9 mm BL were counted individually. In larvae greater than 9 mm BL, ionocytes were counted individually on 10% of the total surface area of the larvae, and that number was extrapolated to estimate the total number of cutaneous ionocytes, a method developed by Kwan et al. (2019). Briefly, a coordinated grid was created, with each square's side accounting for 2% of the BL of the larva. To account for differences in ionocyte density on the head, trunk, and fin regions of each larva, the number of boxes counted in each area was proportional to the area of that region specifically. The squares to count were chosen by a random coordinate generator in R (ver. 0.98.1103) but were discarded if they contained areas

from more than one portion of the larvae, any portion of the eye, any portion containing a glare, an edge of the larval surface, or an invaginated surface such as the first dorsal fin, the pelvic fin, or an opercular fold. This method was validated by comparing estimated numbers to those counted by hand in two different larvae and was found to be ~10% accurate (9.41 mm BL larva: 10,890 estimated, 9,819 counted; 16.40 mm BL larva: 40,733 estimated, 36,516 counted). The average size of ionocytes was determined using the freehand tool in ImageJ to measure the areas of 60 ionocytes; 20 from each of the head, trunk, and fin regions, and dividing the sum of those numbers by 60. Using the total number of cutaneous ionocytes, average ionocyte size, and the total surface area of each individual White Seabass larvae, a "relative ionocyte area" (RIA) was obtained via the following equation:

$$Relative\ Ionocyte\ Area = \frac{(number\ of\ cutaneous\ ionocytes) \times\ (average\ cutaneous\ ionocyte\ area)}{total\ surface\ area}$$

The RIA provides a singular number for each larva that is assumed to represent osmoregulatory capacity on the skin, which can be compared amongst larvae throughout the sample period.

In addition to measuring RIA, change in average ionocyte size within each body region (head, trunk, fins) was measured. Twenty-four larval images were selected based on BL to create a size range from 3.1 mm to 15.3 mm BL, with ~2 larval images per 1 mm change. The average size of ionocytes was determined in a similar fashion as described earlier, by using the freehand tool and dividing the sum of areas by the number of ionocytes measured. The data collected were visualized in two ways: 1) Average size of ionocytes versus body length for each body region, and 2) average size of ionocytes within each body region separated by 4 size classes: 3-6 mm, 6-9 mm, 9-12 mm, 12-16 mm, with each size class including 6 larvae. Plotting change in

ionocyte size based on size class allows for a clearer comparison across the three body regions throughout the entirety of the sample period.

Scanning Electron Microscopy

Apical morphology of ionocytes on the fin, trunk, and gills of larvae from 32 DPH larva were examined using scanning electron microscopy. The fixed larva was first dehydrated in an ascending series of tert-butyl alcohol (tBa). The series consisted of five washes of tBa beginning with a 50% dilution and gradually increasing the concentration of tBa to 100% over two days. Samples were suspended in tBa in glass scintillation vials in an incubator at 35ºC, as tBa has a freezing point of 25.5ºC. After the final wash, tBa was allowed to solidify before being placed in a VirTis Benchtop K freeze-dryer (SP Scientific, Warminster, PA, USA) where it was then sublimated under vacuum (~100mT) at -50ºC overnight. The resulting dehydrated sample was then sputter-coated with gold and viewed using Zeiss EVO MA10 SEM under high-vacuum mode.

RESULTS

Growth and Development

Body length (n=73) increased linearly with age throughout the sample period. White Seabass larvae sampled in this study ranged from 2.61 mm BL at 1 DPH to 16.40 mm BL at 32 DPH. Larvae were in pre-flexion stage at ≤ 6 mm BL, notochord flexion stage between 6 and 7 mm BL, post flexion stage between 7 and 10 mm BL, and transformation stage at ≥ 10 mm BL (Figure 3). Formation of fin rays was first observed at ~6.25 mm BL in the dorsoventral portion of the median finfold. Fin rays were observed throughout the median finfold by ~7 mm BL before the separation of the dorsal, caudal, and anal fins occurred at ~8 mm BL (Figure 5). Gill arches were present at all points throughout the sample period. Gill filaments were first observed at ~3.25 mm BL, and lamellae were first observed at ~4.5 mm BL (Figure 6).

NKA is Present in the Basolateral Membrane of Ionocytes

Western blot with anti-NKA monoclonal antibodies on 32 DPH White Seabass larvae revealed a single ~108 kDa band, matching the predicted size of the protein (Figure 4). The presence of a faint band in the crude homogenate lane, no band in the cytosolic fraction lane, and a dark band in the membrane fraction lane indicate that NKA is highly abundant in the basolateral membrane of the cell.

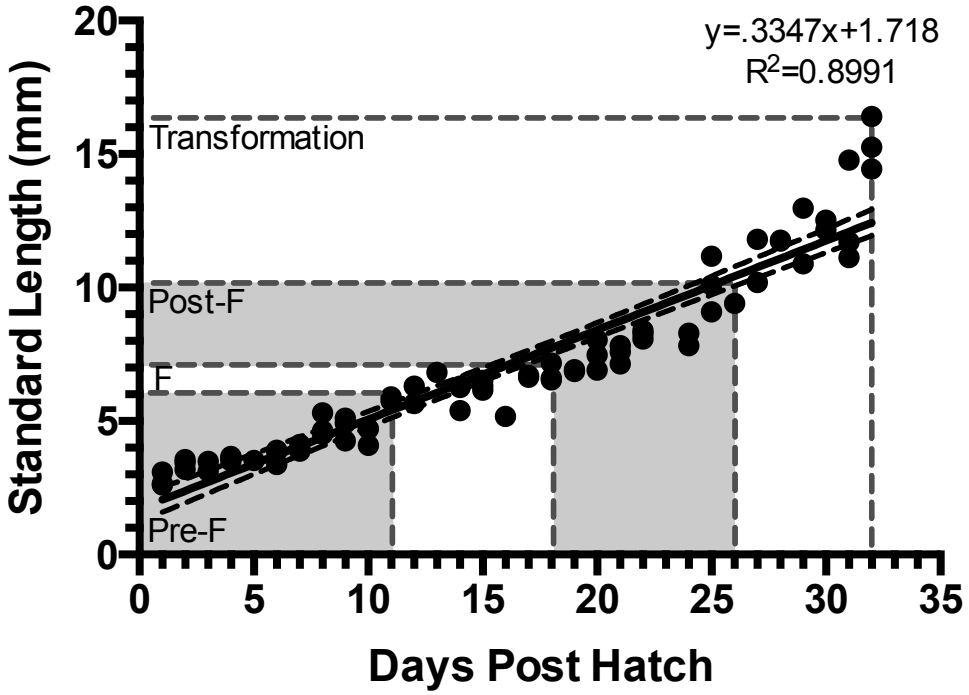

Figure 3: Change in body length in relation to age throughout larval White Seabass development. The black line indicates the linear regression and the dotted line represents the 95% confidence interval. *Pre-F* pre-flexion, *F* flexion, *Post-F* post flexion.

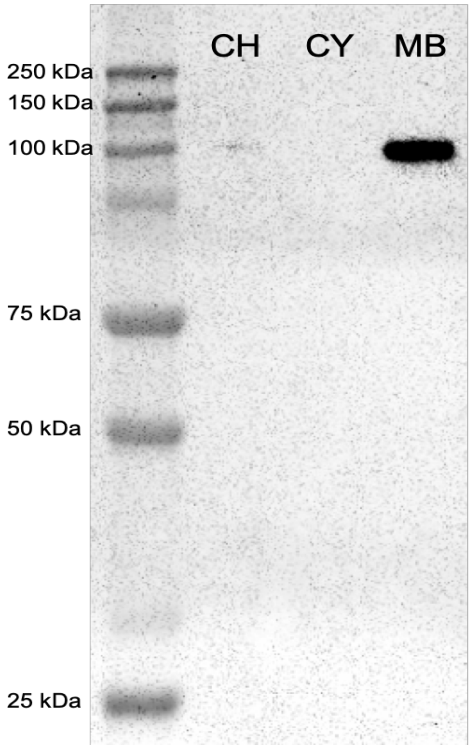

Figure 4: Western blot with anti-NKA monoclonal antibodies. *CH* crude homogenate, *CY* cytosolic fraction, *MB* membrane fraction.

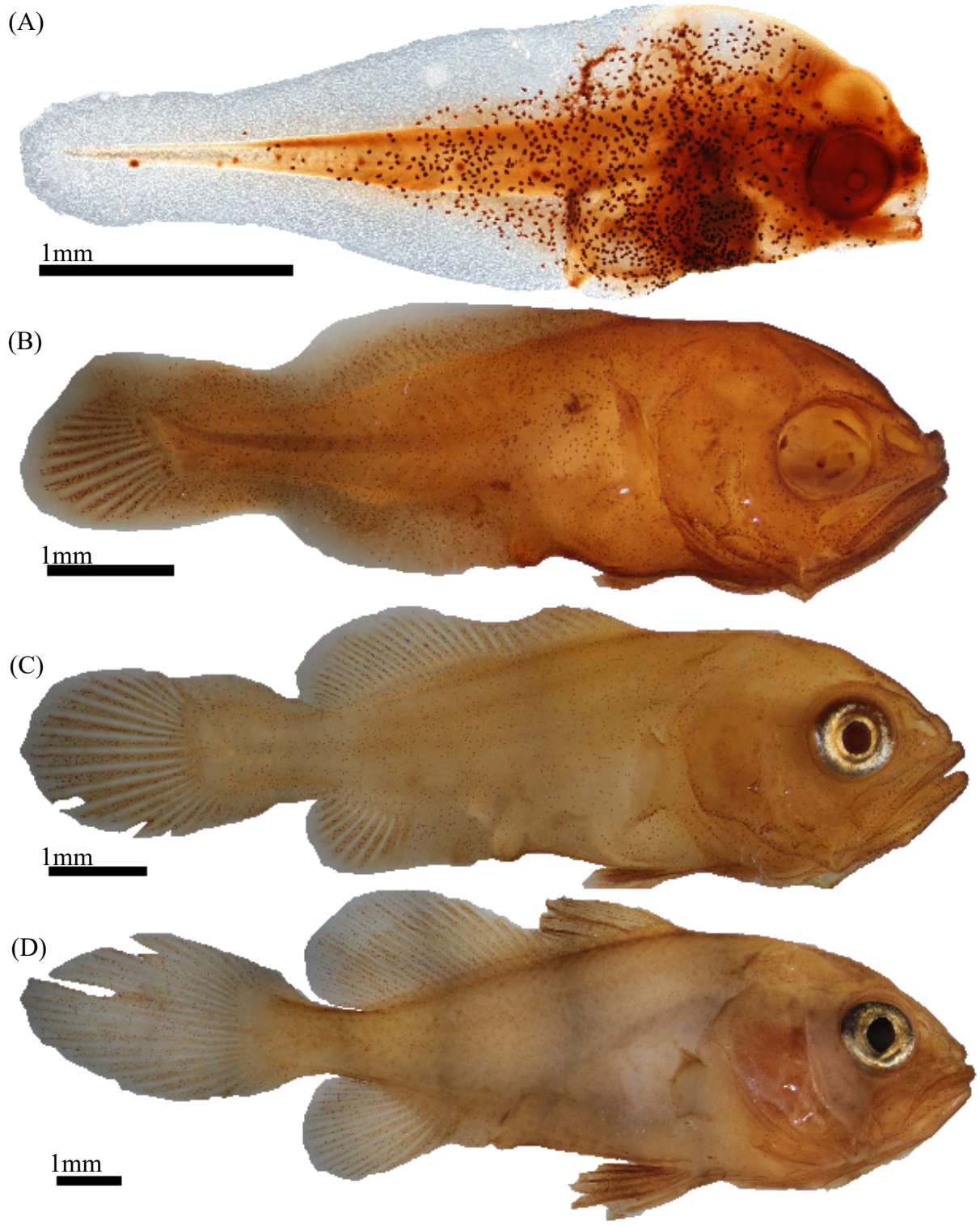

Figure 5: Na^+/K^+ immunostained light microscopy images showing four developmental stages of White Seabass larvae. A) Pre-flexion larvae, 3.49 mm BL (3 DPH). B) Flexion larvae, 6.33 mm BL (15 DPH); note: right eye of larvae was lost during immunostaining process. C) Post-flexion larvae, 7.83 mm BL (21 DPH). D) Transformation larvae, 11.1 mm BL (31 DPH)

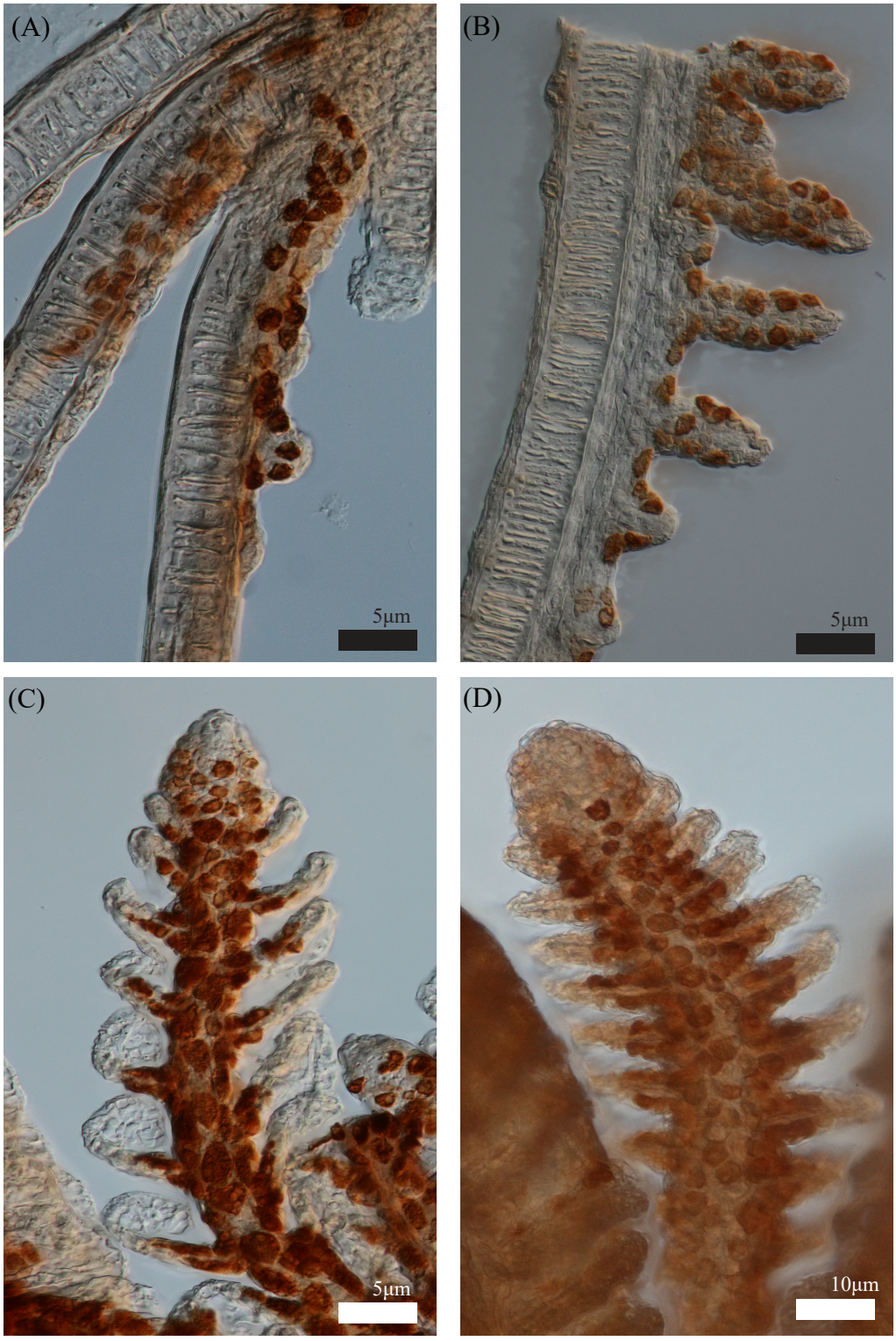

Figure 6: Na^+/K^+ immunostained light microscopy images showing development of branchial structures and presence of ionocytes in a developmental series of White Seabass larvae. A) Newly budding gill filaments emerging from gill arches of a 3.24 mm BL (5 DPH) larva. B) Developing filaments of a 3.71 mm BL (7 DPH) larva. C) Further developed gill filament now with lamellae of a 6.29 mm BL (16 DPH) larva. D) Well developed gill filament and lamellae of a 14.99 mm BL (32 DPH) larva.

Cutaneous ionocyte abundance, size, density, and relative ionocyte area

A biphasic pattern was observed in the number of ionocytes, ionocyte size, and ionocyte density throughout the sample period. Each measure exhibited either an abrupt increase or decrease in the rate of change during notochord flexion. The number of ionocytes increased from a minimum of 1,027 cells at 2.6 mm BL to 38,894 cells at 14.4 mm BL. The number of ionocytes increased gradually, remaining under 2000 cells, until ~6 mm BL when the number of ionocytes then increased at a much higher rate throughout the flexion, post-flexion, and transformation stages (Figure 7). Ionocyte size decreased linearly from 283 μm^2 at 2.6 mm BL when it then plateaued out after ~7 mm BL, remaining between 100 μm^2 and 145 μm^2 through the remainder of the sample period (Figure 8_A). The ionocyte density (measured as number of ionocytes/mm^2) decreased rapidly until ~4.5 mm BL when it then sharply increased throughout the remainder of the sample period (Figure 8_B). RIA also showed a biphasic pattern throughout the sample period, beginning with a rapid decrease during pre-flexion followed by stabilization throughout flexion, post-flexion, and transformation. RIA decreased drastically from 14% at 2.6 mm BL (1 DPH) to 4% at 4.3 mm BL (9 DPH), when it then stabilized, remaining between 3% and 6% throughout the remainder of the sample period (Figure 9).

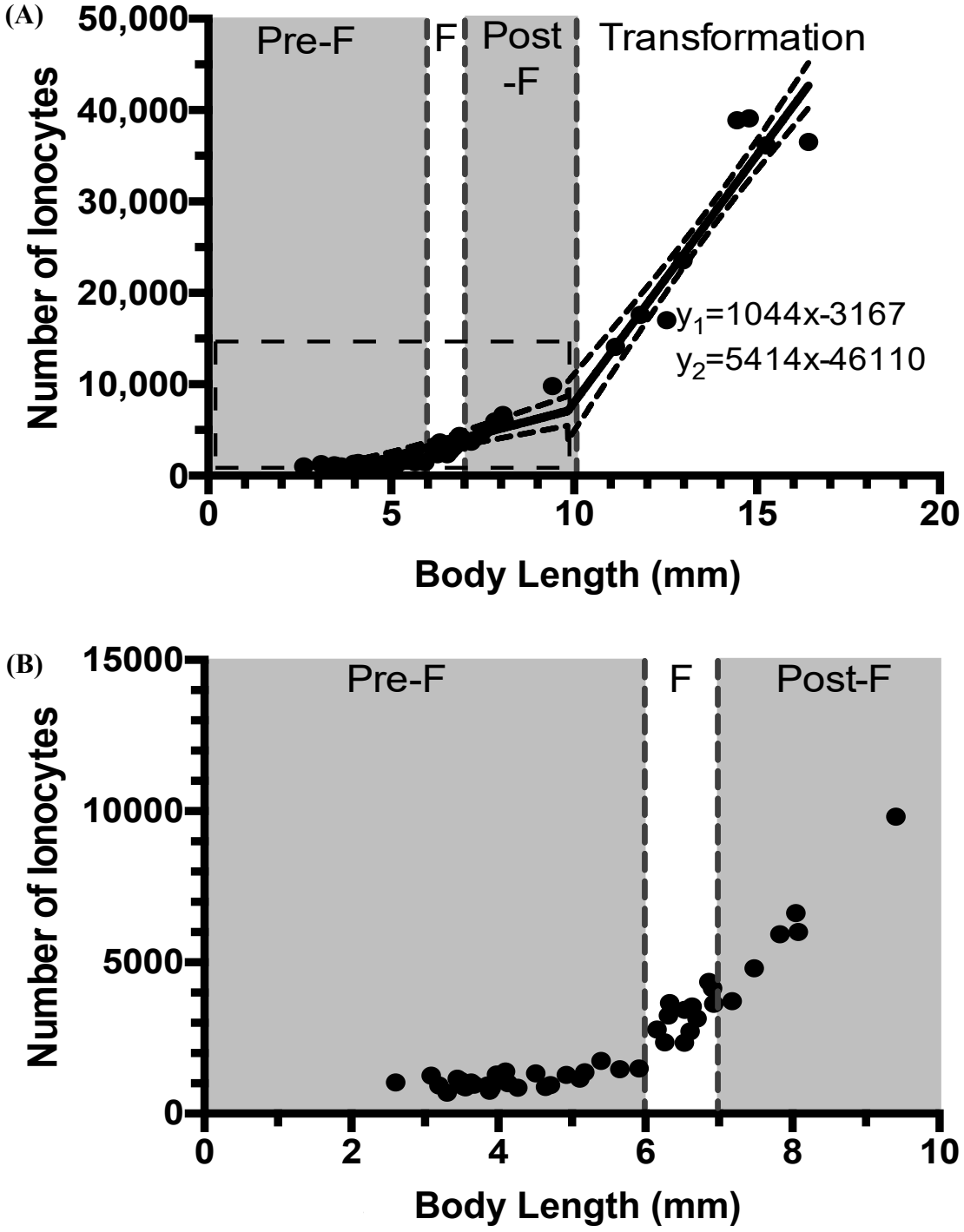

Figure 7: A) Estimated total number of cutaneous ionocytes in larval White Seabass ranging from 2.6 mm to 16.4 mm BL. Dotted lines denote 95% confidence intervals. B) Inlay of dotted box in graph 2A. Regression lines and 95% confidence intervals were removed to provide a clearer view of the rate change occurring around the timing of notochord flexion. *Pre-F* pre-flexion, *F* flexion, *Post-F* post flexion.

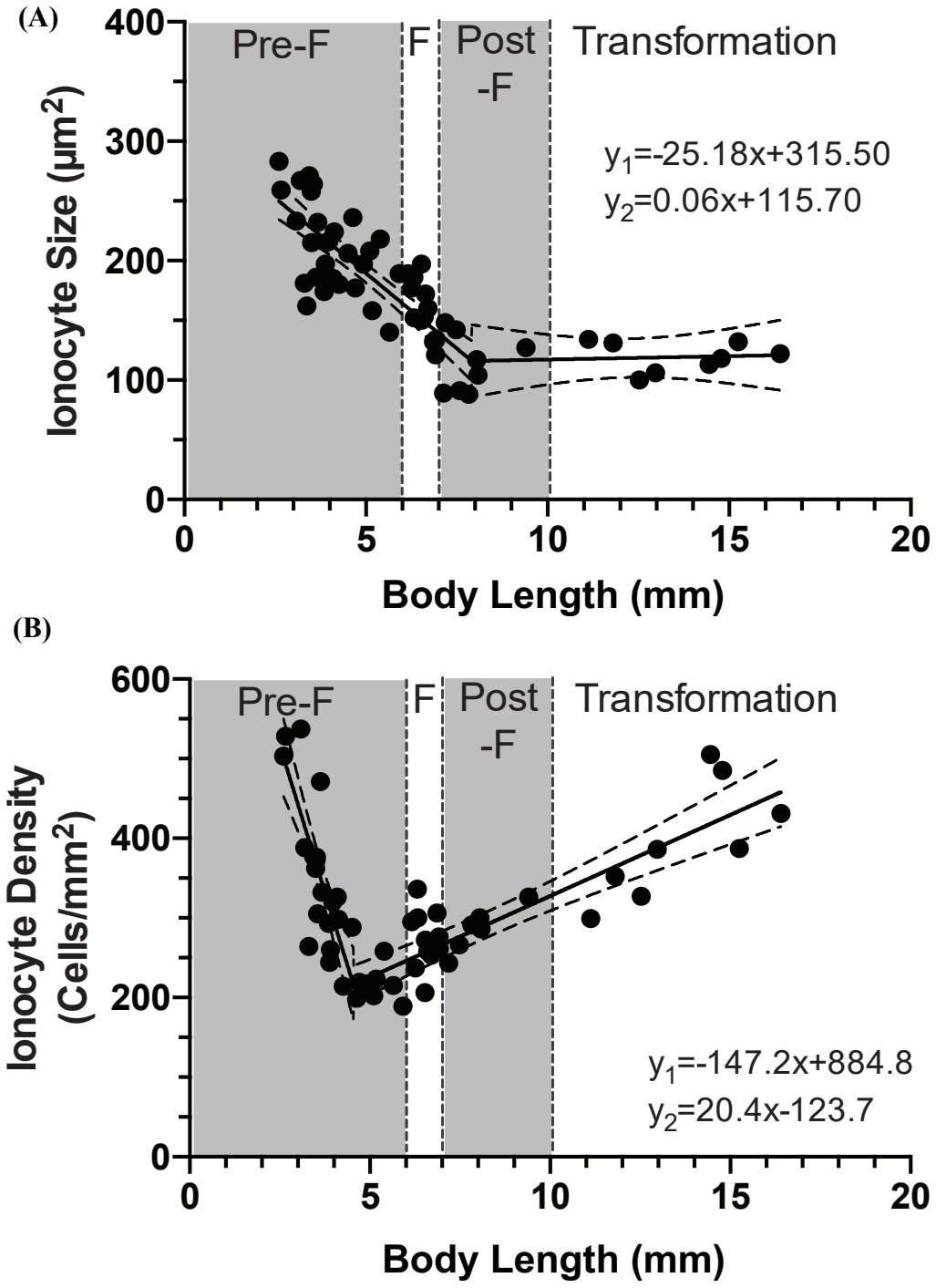

Figure 8: A) Size and B) density of ionocytes in larval White Seabass ranging from 2.6 mm to 16.4 mm BL. Dotted lines denote 95% confidence intervals. *Pre-F* pre-flexion, *F* flexion, *Post-F* post flexion.

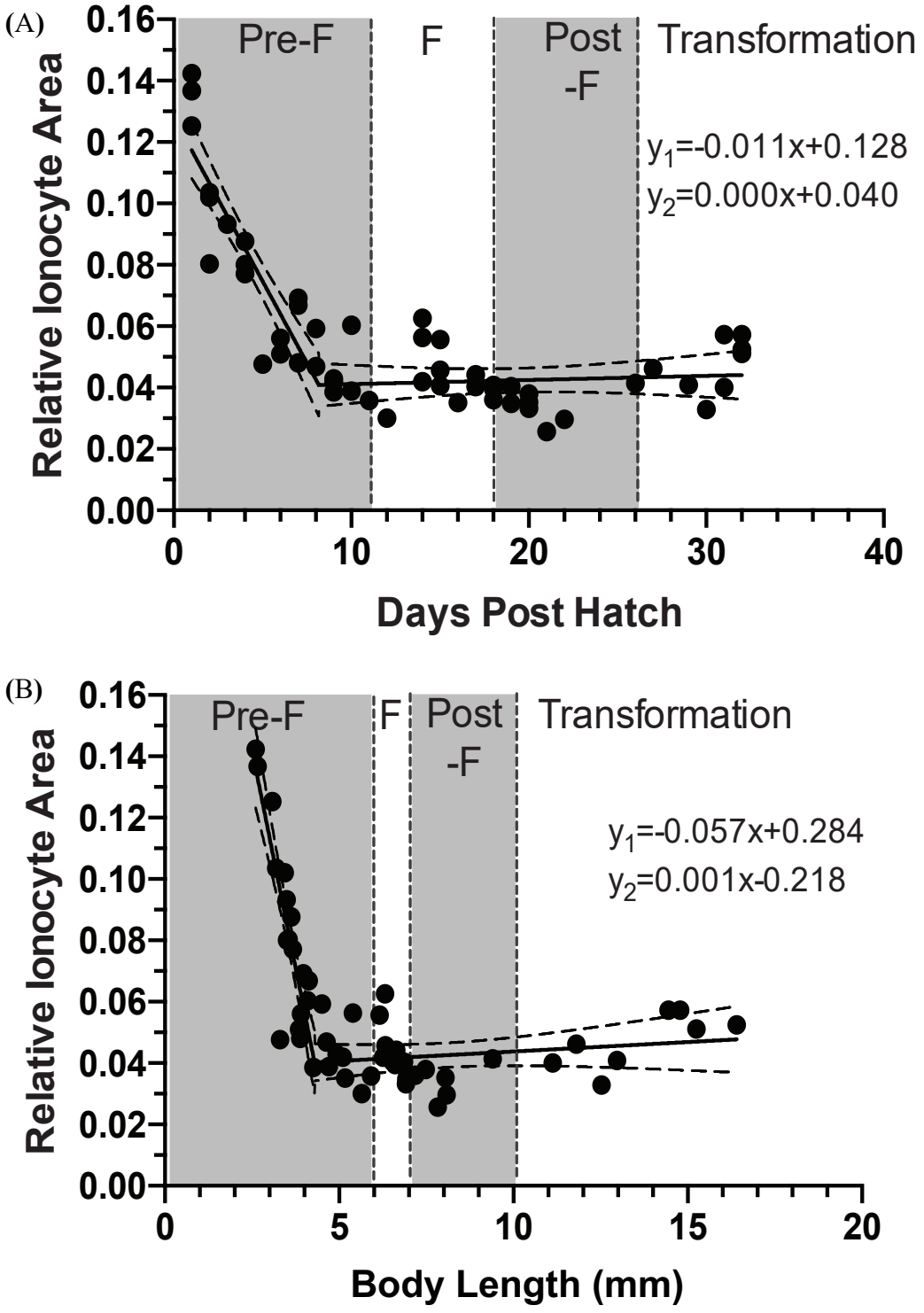

Figure 9: Cutaneous ionocyte area relative to total skin surface area in larval White Seabass ranging from 2.6 mm to 16.4 mm BL in relation to A) days post-hatch and B) body length. Dotted lines denote 95% confidence intervals. *Pre-F* pre-flexion, *F* flexion, *Post-F* post flexion.

Variation in Ionocyte Size in Different Body Regions

Ionocytes in the head and trunk decreased in size until stabilizing after notochord flexion. Ionocytes in the fins decreased in size until notochord flexion, then returned to near their original size by the end of the sample period. Ionocyte size within both the head and trunk regions decreased from ~275 μm^2 in larvae ≤ 7 mm BL, where it then stabilized at ~110 μm^2 for the remainder of the sample period (Figure $10_{A,B}$). Ionocyte size in the fins decreased from ~200 μm^2 to ~75 μm^2 in larvae ≤ 7 mm BL, where it then increased, returning to ~200 μm^2 by the end of the sample period. (Figure 10_C). The data was binned into four size groups: 3-5 mm, 6-8 mm, 9-11 mm, and 12-15 mm BL. Ionocytes in all three regions decreased in size in the 3-5 and 6-8mm groups. Only the ionocytes in the fins increased in size in the 9-11 and 12-15mm groups, (Figure 11).

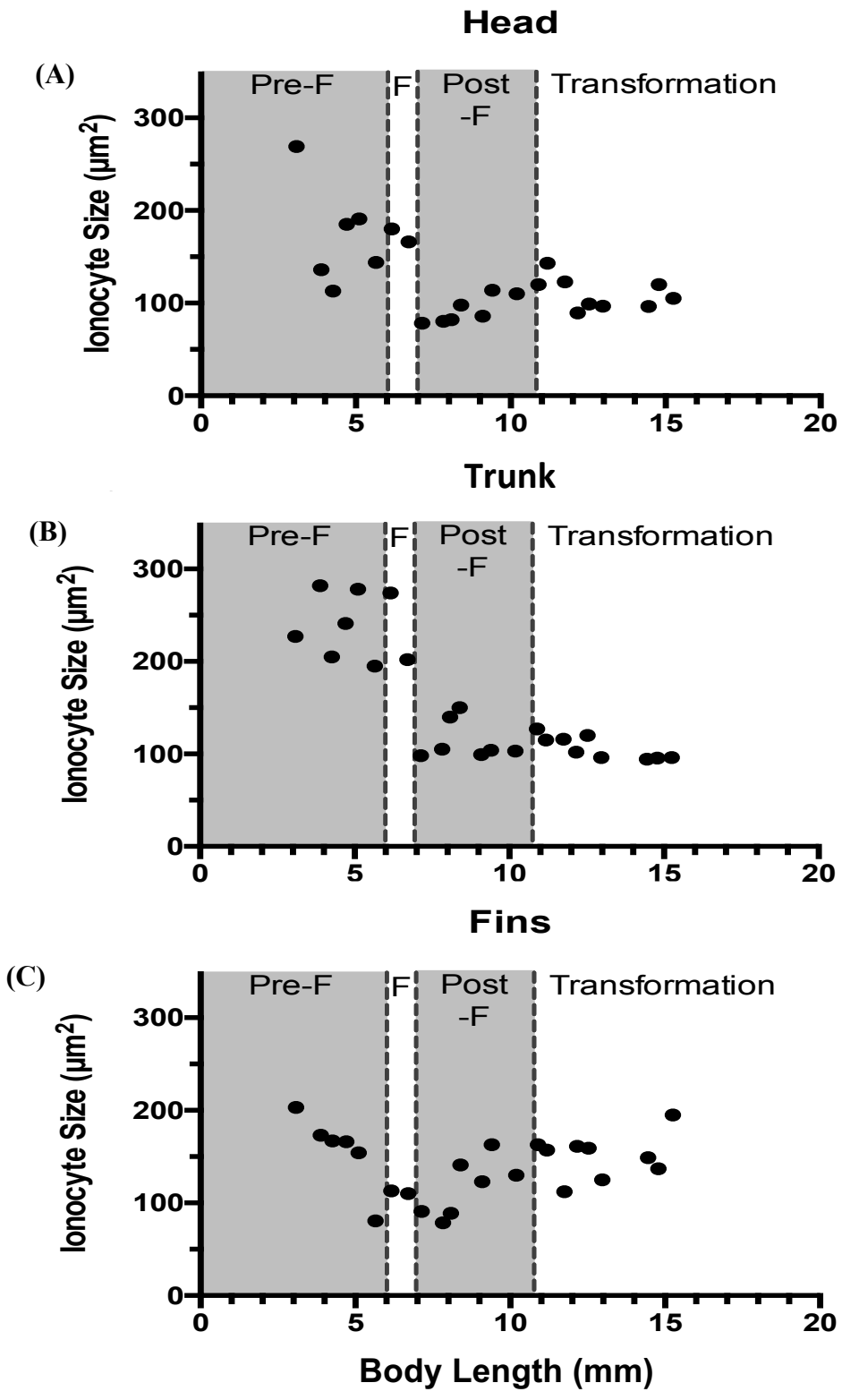

Figure 10: Change in ionocyte size in the A) head, B) trunk, and C) fins in larval White Seabass ranging from 2.6 mm to 16.4 mm BL. *Pre-F* pre-flexion, *F* flexion, *Post-F* post flexion.

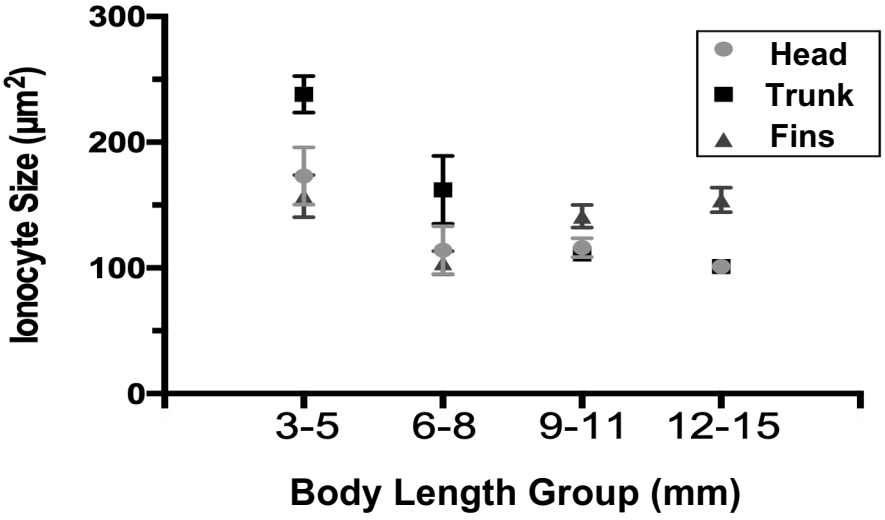

Figure 11: Differences in ionocyte size between head, trunk, and fin regions of White Seabass larvae in 3-5 mm BL, 6-8 mm BL, 9-11 mm BL, and 12-15 mm BL size groups. Grey circles denote average size of head ionocytes, black squares denote average size of trunk ionocytes, dark grey triangles denote average size fin ionocytes.

Variation in ionocyte apical membrane morphology

SEM imaging of ionocytes of a transformation stage larva (32 DPH, 16.10 mm BL) revealed morphological differences in the apical membrane of gill ionocytes in comparison to the trunk and fin ionocytes. Ionocytes in the trunk and fins exhibited deepened apical pits with retracted microvilli and were generally < ~5µm in diameter at the widest (Figure $12_{A,B}$). Ionocytes on the gill filaments exhibited wide, shallow apical membranes with extended microvilli and were generally > 5µm in diameter at the widest (Figure 12_{C}). Ionocytes were expected to be observed on the basal portion of the lamellae but were only observed the trailing edge of the filaments. The lamellae, and the larva in general, appeared dehydrated. I expect this is likely product of the SEM fixation process which requires further optimization.

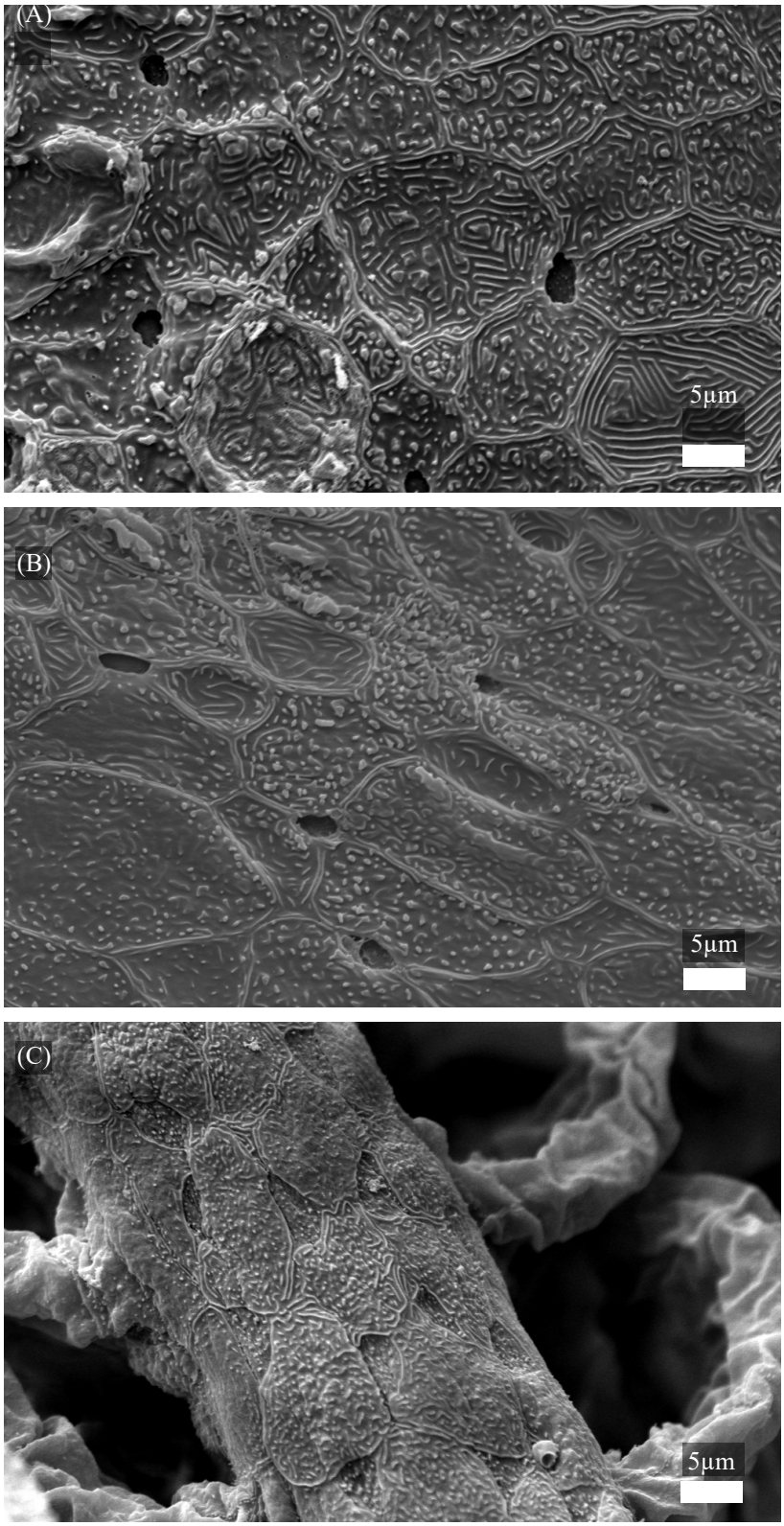

Figure 12: SEM images of apical membrane morphologies of A) skin, B) fin, and C) gill ionocytes of a 32 DPH, 16.10mm BL White Seabass larva. Black arrows indicate ionocytes with apical pits, white arrows indicate ionocytes with widened apical pits and extended microvilli.

Cutaneous Ionocytes on the Skin of Juvenile White Seabass

The skin of a ~6-month old White Seabass, hatched at HSWRI and raised in an experimental aquarium at Scripps Institution of Oceanography was examined using CLSM, revealing an abundance of ionocytes present on the skin well past the larval stage. Differential interference contrast (DIC) revealed the apical morphology of pavement cells and ionocytes with ~5 µm wide apical pits scattered throughout the skin (Figure 13_{A}). The basolateral membrane of ionocytes were identified by intense red fluorescence from NKA immunolabelling, revealing an elongated columnar cell morphology extending from ~3-25 µm below the surface of the epithelium (Figure $13_{B, D}$). NKA was not present in the apical membrane of the ionocyte (Figure $13_{A, E, F}$). Average ionocyte sizes, numbers, densities, and RIAs were not determined in this sample. Rather, this was a short exploratory work to determine whether or not ionocytes remained present in the skin of White Seabass beyond larval stages.

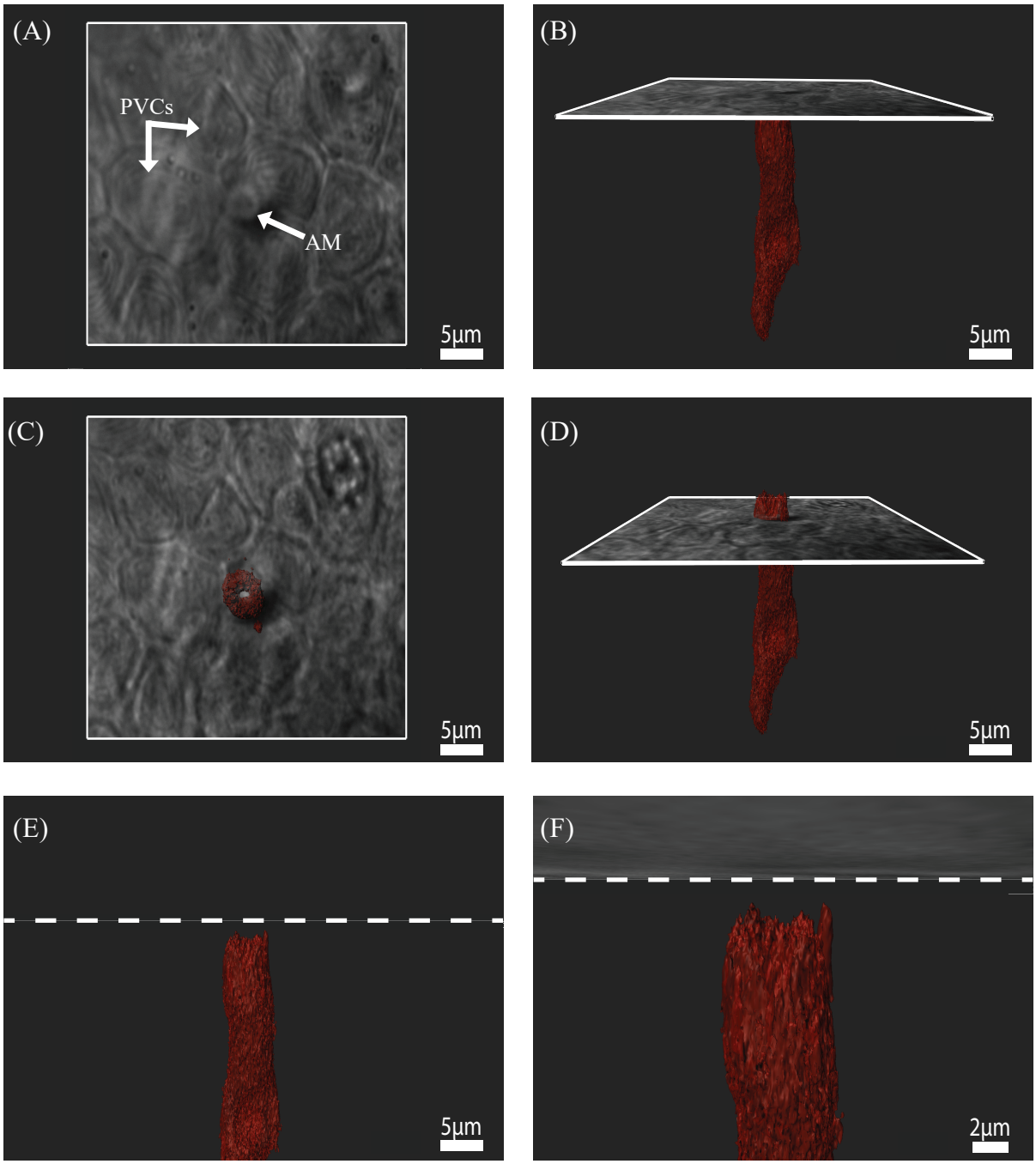

Figure 13: Three-dimensional rendering of NKA immunostaining of an ionocyte on the skin of a juvenile White Seabass. Red coloration indicates presence of NKA. Note that NKA is only present in the basolateral membrane of the cell. (A) DIC view of the apical morphology of pavement cells and apical membrane of an ionocyte. *PVCs* pavement cells, *AM* apical membrane. (B) Lateral view of the ionocyte. The white square indicates where the overhead view from (A) was captured. (C) DIC view 5µm below the depth at which (A) was captured. (D) Lateral view of the ionocyte and location of overhead view from (C). (E) and (F) Lateral view indicating that NKA is only present in the basolateral membrane of the cell. White dotted line indicates location of the apical membrane, at the depth which (A) was captured.

DISCUSSION

Here I present the first data tracking ontogenetic changes in ionocytes in larval White Seabass. RIA was highest in the youngest larvae, sharply decreased during the pre-flexion stage until just prior to notochord flexion, and then remained constant through the rest of the sample period. Since RIA is a measure of ion transporting capacity across the skin, these results indicate a progressive decrease in the involvement of the skin in osmoregulation (and possibly acid/base regulation and NH_3 excretion) as larvae develop into juveniles. It was also observed that the size of ionocytes in the head and trunk progressively decreased, while fin ionocytes first decreased, then increased in size, following flexion and the appearance of fin rays. A variety of ionocyte apical membrane morphologies were observed in a 32 DPH, transformation stage larva. Ionocytes did not disappear from the skin by the end of the sample period, and many were still present on the skin of a 6-month old juvenile White Seabass. This indicates that the skin is involved in ion transporting processes throughout larval metamorphosis and beyond.

Growth/Development

White Seabass growth rates and the timing of developmental events in my study were generally similar to those reported by Moser et al. (1983), which provides the most detailed description of the early life stages of White Seabass to date, although the larvae in this study grew at a slightly faster rate. Differences in temperature likely contributed to growth rate discrepancies observed between the two studies. While the experiments by Moser et al. (1983) were conducted in temperatures ranging from 16.5 to 20^{o}C, my study raised larvae in a narrower temperature range of 19.0-19.6°C. While variation arose in BL-age relationships, the timing of important developmental events, such as notochord flexion, occurred at similar body lengths in both studies. In White Seabass larvae, notochord flexion marks the timing of the median fin fold

separating into the dorsal, anal, and caudal fins, an enlargement of paired fins, rapid development of the head, jaw, and eyes, ossification of fin rays, and the formation of the digestive tract (Galaviz et al., 2011; Moser et al., 1983). In my study, notochord flexion also coincides with a decrease in skin RIA and the formation of branchial structures important for gas exchange and ion transport.

Changes in Cutaneous and Branchial Ionocyte Abundance and Localization

Cutaneous ionocytes experienced numerous significant changes around the notochord flexion stage: they cease to decrease in size, their numbers begin to increase at a higher rate, and they switch from decreasing to increasing density. However, none of these metrics accurately reflect cutaneous ion transporting capacity when examined individually. Instead, RIA was calculated to take into account the effect of both the number and size of ionocytes in relation to the body size of each larvae. RIA relies on immunolabelling of NKA, and this enzyme is present in the ionocyte basolateral membrane. Thus, RIA is not a measure of the body *surface* occupied by ionocytes, but instead a proxy for ion transporting capacity related to NKA in the highly infolded basolateral membranes of ionocytes. I calculated RIA for each larva to examine ion transport capacity across the skin throughout larval development.

White Seabass larvae in this study underwent a drastic reduction in RIA during the first ~10 DPH, until reaching ~4 mm BL where RIA ceased to decrease (Figure 9). Considering RIA in the context of ion transport capacity, these data suggest that more ion transport is occurring across the skin in pre-flexion larvae in comparison to later life stages. The surface area to volume (SA/Vol) ratio of pre-flexion larval White Seabass is low enough that sufficient ion transport can take place across the skin to maintain homeostasis. As White Seabass larvae increase in size, their SA/Vol ratio decreases, and they can no longer perform sufficient gas and ion exchange

across the skin. The development of gills increases the amount of total surface area, making up for the decrease in SA/Vol. White Seabass larvae during pre-flexion lack well developed branchial structures, with filaments and lamellae not appearing until ~5 and 10 days post hatch, respectively, just before the timing of notochord flexion (Figure 6). During notochord flexion, a rapid development of branchial structures was observed that continued throughout the sample period.

Ionocytes were present on gill arches of larvae as early as 5 DPH, the smallest larvae in which gill extraction was successful (Figure 6_A). However, the high abundance of ionocytes at this point suggest that ionocytes are likely present on the arches before 5 DPH. Gill filaments were first detected at 5 DPH (Figure 6_A). Although in a very rudimentary form, the early-filaments were already abundantly covered by ionocytes. Lamellae first appeared on the filaments between 8-10 DPH, and ionocytes were present on the basal portion of the lamellae (Figure $6_{C, D}$). This localization is different from previous reports of ionocytes located primarily in gill filaments of seawater acclimated diadromous and euryhaline fishes. In juvenile Alewives (*Alosa pseudoharengus*), lamellar ionocytes decreased in abundance by 85% during a 2-week acclimation from fresh to seawater (Christensen, 2012). In juvenile American Shad (*Alosa sapidissima*), lamellar ionocytes disappeared entirely after a 10-day acclimation from fresh to seawater (Zydlewski & McCormick, 2001). Lamellar ionocytes were absent in seawater acclimated Japanese Seabass, but were abundantly present after a 10-day exposure to freshwater (Inokuchi et al., 2017). More examples of salinity effects on branchial ionocyte localization in euryhaline teleosts are reviewed in Hiroi & McCormick, 2012, but overall the data generally suggest that ionocytes are only present on lamellae during freshwater exposure.

Less data exist focusing on branchial ionocyte localization in exclusively marine species. To my knowledge, only two studies exist which examined in detail the presence or absence of ionocytes on the filaments and lamellae of marine teleosts. Ionocytes were observed on both the filament and lamellae of adult Pipefish (*Sygnathus schlegeli*) [Watanabe et al., 1999], and were present on the filament but not the lamellae of larval Yellowfin Tuna (*Thunnus albacares*) [Kwan, 2018]. Ionocyte localization on the base of lamellae in larval White Seabass, is unique in comparison to these studies. Future studies should explore the effects of altered pH, salinity, and dissolved oxygen concentrations on the distribution of gill ionocytes in White Seabass and other marine teleost larvae, using this study as a baseline.

It is important to note that while RIA did show a marked decrease from hatch to the end of the sample period of this study, ionocytes are still present in the skin of White Seabass well beyond the larval stage (Figure 13). The skin of juvenile White Seabass (~6 months age) immunostained for NKA and examined using confocal scanning laser microscopy indicated an abundance of ionocytes on the skin of the trunk region of the body. These data agree with previous works in which ionocytes have been identified on the skin of other juvenile and adult teleost species including the marine Long Jawed Mudsucker (*Gillichthys mirabilis*) [Marshall & Nishioka, 1980] and Shanny (*Lipophrys pholis*) [Nonnotte, 1979] as well as seawater-acclimated Mummichog (*Fundulus* heteroclitus) [Degnan, 1977] and Marbled Swamp Eel (*Synbranchus marmoratus*) [Stiffler, 1985]. Cutaneous ion transport via ionocytes has been reported in a variety of additional teleost species (further reviewed in Glover et al, 2013). Future work could utilize White Seabass as a marine species to explore the skin's role in osmoregulation, as well as responses to acid/base, ammonia, salinity, and reduced oxygen stressors.

Ionocytes in all measured regions decreased in size from hatch until ~6-7 mm BL, corresponding to the timing of notochord flexion. From this point on, ionocytes in the head and trunk remained at a relatively constant size, while the fin ionocytes increased in size throughout the remainder of the sample period (Figure 10). Following notochord flexion, fin rays begin to rapidly develop throughout the length of the median fin fold (Figure 5). A potential explanation for the increase in ionocyte size in the fins during this time is they may be playing a more active physiological role in the biomineralization of fin rays. Biomineral formation requires a localized zone that contains biomineral constituents, primarily Ca^{2+} and phosphates in the case of vertebrates, and a pH above ~7.4 (Arnett, 2008; Beck, 2019; Weiner, 2003). The direct relationship between ionocyte density and cutaneous epithelial Ca^{2+} uptake observed in the freshwater Nile Tilapia (*Oreochromis niloticus*) [Marshall et al., 1992] and rainbow trout (*O. mykiss*) [McCormick et al., 2006] indicates a role for ionocytes in Ca^{2+} homeostasis. However, Ca^{2+} concentrations are low in freshwater compared to seawater, averaging ~0.07mM and ~9.6mM, respectively (Evans, 2005), so it is not clear if marine teleosts require similar cutaneous epithelial Ca^{2+} uptake mechanisms as freshwater teleosts. In addition, to Ca^{2+} uptake, ionocytes are known to be involved in acid secretion. The acid secreting proteins NHEs can be found in the apical membrane of some ionocytes in both freshwater and marine species (reviewed in Evans, 2005 and Hwang, 2011). Thus, fin ionocytes may play a role in biomineralization both supplying calcium and maintaining pH above 7.4 in zones of calcification. Further exploration into the physiological capabilities of ionocytes to aid in biomineralization using immunohistochemical labelling of known biomineralization proteins (e.g. NHE, PMCA2, NCX1b) are needed.

Variation in apical membrane morphology of ionocytes

The apical morphology of ionocytes has been observed to be able to change dramatically. In juvenile Killifish (*Fundulus heteroclitus*) [Katoh et al. 2002] and adult European Seabass (*Diccentrarchus labrax*) [Vasamos, 2002], apical membranes of gill ionocytes were observed to change in response to varying salinities. In both species, apical membranes formed pits in response to high [NaCl] exposure, but became widened and shallow with extended microvilli in response to low [NaCl] exposure. This data suggests that the morphology of gill ionocytes change in order to provide additional surface area for ion exchange in freshwater conditions. Similarly, ionocytes of larval Yellowfin Tuna (*T. albacarus)* [Kwan, 2018] changed throughout larval metamorphosis. Apical membranes of skin ionocytes were widened with extended microvilli in pre-flexion larvae and formed pits in post-flexion larvae. In transformation stage larvae, apical membranes of gill ionocytes exhibited widened pits with extended microvilli, while apical membranes of skin ionocytes exhibited apical pits. This data suggests that increasing apical membrane surface area is a regulatory mechanism to increase ion excretion in yellowfin tuna larvae. As the larvae develop, apical membranes of ionocytes on the skin form pits, likely indicating a reduction in ion excretion as the gills become increasingly developed.

In addition to tracking ionocyte localization and morphology through the use of immunohistochemistry, this study used SEM to determine if White Seabass larvae exhibit different ionocyte apical morphologies in different regions of the body. It was observed that ionocytes on the gills of a 32 DPH (16.10 mm SL) larva exhibited widened apical membranes and extended microvilli (Figure 12_{C}) in comparison to ionocytes on the trunk and fins, which exhibited apical pits (Figure $12_{A,B}$). However, the low sample size and poor condition of the

larva examined (likely a byproduct of the fixation process) prevented making any reliable conclusions. Regardless, the apparent differences in ionocyte apical morphologies in transformation stage larvae suggest these cells may be exhibiting different activity levels, performing different functions, or may constitute different ionocyte subtypes entirely.

Conclusions and Future Work

It was shown that a shift of osmoregulatory capacity from the skin to the gills corresponded to the timing of notochord flexion in larval White Seabass. A rapid decrease in relative ionocyte area from ~14% to ~4% occurred just prior to notochord flexion, where it then remained between 3% and 6% throughout the remainder of the sample period. At this same time, branchial structures with abundant ionocytes became increasingly developed. The decrease in relative ionocyte area on the skin appears to correlate to the branchial structures taking on a large portion of osmoregulatory load. It was also observed that ionocytes on the fins were significantly larger than those on the body and the head in later stage larvae, but the underlying reasons remain unclear. Ionocytes displayed varying apical membrane morphologies in the skin of the trunk and fin regions in comparison to those on those on the gills, which exhibited widened apical membranes, suggesting these ionocytes vary in activity, function, or cell sub-type. While the gills appear to take on the bulk of ion transport processes in later stage larvae, the presence of ionocytes on the skin of a 6-month old juvenile White Seabass indicates that the skin likely still plays a role in ion transport well beyond the larval stage.

This study is the first to track the functional transition of ionocytes from the skin to the gills in larval White Seabass. In comparison to similar studies on ionocytes in marine teleost larvae, there appears to be distinct differences between species in relation to the rate of transition

of ionocyte abundance from the skin to the gills, and the localization of ionocytes on the gill lamellae. This study established a baseline in the functional transition of ionocytes from the skin to the gills in larval White Seabass raised in typical aquaculture conditions, and can be used in future studies exploring the effects of altered pH, temperature, salinity, and dissolved oxygen on ion transport capacity on the skin and gills of marine teleost larvae. If such stressors have an effect on the distribution, morphology, or function of ionocytes, the ability for larval teleosts to maintain homeostasis, and therefore survive, will likely be altered. This has broad implications and a high socioeconomic value for the aquaculture and fisheries industries, and can be taken into account in climate studies that have a focus on biological responses. More work is required to explore functional reasoning as to why ionocytes on the fins remain larger than other regions of the body in later stage larvae, and further work should be invested into characterizing the different apical morphologies of ionocytes in relation to their function. Lastly, I suggest the skin should not be ignored as a key player in osmoregulation, acid base regulation, and other ion transport functions in juvenile and adult marine teleosts, as the abundance of ionocytes there may implies it plays a much larger role than what is generally believed.

REFERENCES

Aalbers, S. A., & Sepulveda, C. A. (2015). Seasonal movement patterns and temperature profiles of adult White Seabass (Atractoscion nobilis) off California. *Fishery Bulletin*, *113*(1), 1–14. https://doi.org/10.7755/FB.113.1.1

Allen, L. G., Pondella, D. J., & Shane, M. A. (2007). Fisheries independent assessment of a returning fishery: Abundance of juvenile White Seabass (Atractoscion nobilis) in the shallow nearshore waters of the Southern California Bight, 1995-2005. *Fisheries Research*, *88*(1–3), 24–32. https://doi.org/10.1016/j.fishres.2007.07.012

Allen, L. G., & M. P. Franklin. (1992). Abundance, distribution, and settlement of young-of-the-year White Seabass (Atractoscion nobilis) in the Southern California Bight. *U.S. National Marine Fisheries Service Fishery Bulletin* 90:633–641.

Arnett, T. R. (2008). Extracellular pH Regulates Bone Cell Function. *The Journal of Nutrition*, *138*(2), 415S-418S. https://doi.org/10.1093/jn/138.2.415s

Beck, L. (2019). Expression and function of Slc34 sodium–phosphate co-transporters in skeleton and teeth. *Pflugers Archive European Journal of Physiology*, *471*(1), 175–184. https://doi.org/10.1007/s00424-018-2240-y

California Cooperative Oceanic Fisheries Investigations (CalCOFI) Report, Volume 47. December 2006, Chapter I, 29. https://www.calcofi.org/publications/calcofireports/v47/CalCOFI_Rpt_Vol_47_2006.pdf

Chen, X. L., Zhang, B., Chng, Y. R., Ong, J. L. Y., Chew, S. F., Wong, W. P., Lam, S.H., Ip, Y. K. (2017). Na+/H+ exchanger 3 is expressed in two distinct types of ionocyte, and probably augments ammonia excretion in one of them, in the gills of the climbing perch exposed to seawater. *Frontiers in Physiology*, *8*(NOV), 1–16. https://doi.org/10.3389/fphys.2017.00880

Christensen, A. K., Hiroi, J., Schultz, E. T., & McCormick, S. D. (2012). Branchial ionocyte organization and ion-transport protein expression in juvenile alewives acclimated to freshwater or seawater. *Journal of Experimental Biology*, *215*(4), 642–652. https://doi.org/10.1242/jeb.063057

Degnan, K. J., Karnaky, K. J., & Zadunaisky, J. A. (1977). Active chloride transport in the *in* vitro opercular skin of a teleost (Fundulus herteroclitus), a gill-like epithelium rich in chloride cells. *Journal of Physiology*, (271), 155-191.

Evans, D. H., Piermarini, P. M., & Choe, K. P. (2005). The multifunctional fish gill: Dominant site of gas exchange, osmoregulation, acid-base regulation, and excretion of nitrogenous waste. *Physiological Reviews*. https://doi.org/10.1152/physrev.00050.2003

Fielder, D. S., & Bardsley, W. (1999). A Preliminary Study on the Effects of Salinity on Growth

and Survival of Mulloway Argyrosomus japonicus Larvae and Juveniles. *Journal of the World Aquaculture Society*, *30*(3), 380–387.

Flik, G., Verbost, P. M., & Bonga, S. E. W. (1995). Calcium Transport Processes in Fishes. *Fish Physiology*, *14*(C), 317–342. https://doi.org/10.1016/S1546-5098(08)60251-4

Galaviz, M. A., García-Gasca, A., Drawbridge, M., Álvarez-González, C. A., & López, L. M. (2011). Ontogeny of the digestive tract and enzymatic activity in White Seabass, Atractoscion nobilis, larvae. *Aquaculture*, *318*(1–2), 162–168. https://doi.org/10.1016/j.aquaculture.2011.05.014

Glover, C. N., Bucking, C., & Wood, C. M. (2013). The skin of fish as a transport epithelium: A review. *Journal of Comparative Physiology B: Biochemical, Systemic, and Environmental Physiology*, *183*(7), 877–891. https://doi.org/10.1007/s00360-013-0761-4

Hiroi, J., Kaneko, T., Seikai, T., & Tanaka, M. (1998). Developmental Sequence of Chloride Cells in the Body Skin and Gills of Japanese Flounder (Paralichthys olivaceus) Larvae, *460*, 455–460.

Hiroi, J., & McCormick, S. D. (2012). New insights into gill ionocyte and ion transporter function in euryhaline and diadromous fish. *Respiratory Physiology and Neurobiology*, *184*(3), 257–268. https://doi.org/10.1016/j.resp.2012.07.019

Hubbs SeaWorld Research Institute (HSWRI). *Facilities*. Retrieved from https://hswri.org/facilities/

Hwang, P., Lee, T., & Lin, L. (2011) Ion regulation in fish gills: recent progress in the cellular and molecular mechanisms. *American Journal Physiology, Regulatory, Integrative and Comparative Physiology, 301*(1), R28-R47.

Inokuchi, M., Nakamura, M., Miyanishi, H., Hiroi, J., & Kaneko, T. (2017). Functional classification of gill ionocytes and spatiotemporal changes in their distribution after transfer from seawater to freshwater in Japanese seabass. *The Journal of Experimental Biology*, *220*(24), 4720–4732. https://doi.org/10.1242/jeb.167320

Keys, A., & Willmer, E. N. (1932). “Chloride secreting cells” in the gills of fishes, with special reference to the common eel. *The Journal of Physiology, LXXVI*(3), 368-379.

Kwan, G., Finnerty, S., Wegner, N., & Tresguerres, M. (2019). Quantification of Cutaneous Ionocytes in Small Aquatic Organisms. *Bio-Protocol*, *9*(9), 1–22. https://doi.org/10.21769/BioProtoc.3227

Kwan, G. T., Wexler, J. B., Wegner, N. C., & Tresguerres, M. (2018). Ontogenetic changes in cutaneous and branchial ionocytes and morphology in yellowfin tuna (Thunnus albacares) larvae. *Journal of Comparative Physiology B*, *0*(0), 0. https://doi.org/10.1007/s00360-018-1187-9

Lin, C. H., & Hwang, P. P. (2016). The control of calcium metabolism in zebrafish (Danio rerio). *International Journal of Molecular Sciences*, *17*(11). https://doi.org/10.3390/ijms17111783

Liu, S.-T., Tsung, L., Horng, J.-L., & Lin, L.-Y. (2013). Proton-facilitated ammonia excretion by ionocytes of medaka (Oryzias latipes) acclimated to seawater . *American Journal of Physiology-Regulatory, Integrative and Comparative Physiology*, *305*(3), R242–R251. https://doi.org/10.1152/ajpregu.00047.2013

Marshall, W S, Bryson, S. E., & Wood, C. M. (1992). Calcium transport by isolated skin of rainbow trout. *The Journal of Experimental Biology*, *166*, 297–316. Retrieved from http://www.ncbi.nlm.nih.gov/pubmed/1602278

Marshall, William S., & Nishioka, R. S. (1980). Relation of mitochondria-rich chloride cells to active chloride transport in the skin of a marine teleost. *Journal of Experimental Zoology*, *214*(2), 147–156. https://doi.org/10.1002/jez.1402140204

McCormick, S. D., Hasegawa, S., & Hirano, T. (2006). Calcium uptake in the skin of a freshwater teleost. *Proceedings of the National Academy of Sciences*, *89*(8), 3635–3638. https://doi.org/10.1073/pnas.89.8.3635

Moser, G. H., Ambrose, D. A., Busby, M. S., Butler, J. L., Sandknop, E. M., Sumida, B. Y., & Stevens, E. G. (1983). Description of early stages of White Seabass, atractoscion nobilis, with notes on distribution. CalCOFI Report, XXIV.

Nonnotte, G., Nonnotte, L., & Kirsch, R. (1979). Chloride cells and chloride exchange in the skin of a sea-water teleost, the shanny (Blennius pholis). *Cell and Tissue Research*, *199*(3), 387–396. https://doi.org/10.1007/BF00236077

Ocean Resources Education and Hatchery Program (OREHP). *California Department of Fish and Wildlife*. Retrieved from https://www.wildlife.ca.gov/Conservation/Marine/ABMP/OREHP

Roa, J. N., Munévar, C. L., & Tresguerres, M. (2014). Feeding induces translocation of vacuolar proton ATPase and pendrin to the membrane of leopard shark (Triakis semifasciata) mitochondrion-rich gill cells. *Comparative Biochemistry and Physiology -Part A : Molecular and Integrative Physiology*, *174*, 29–37. https://doi.org/10.1016/j.cbpa.2014.04.003

Roa, J. N., & Tresguerres, M. (2017). Bicarbonate-sensing soluble adenylyl cyclase is present in the cell cytoplasm and nucleus of multiple shark tissues. *Physiological Reports*, *5*(2), 1–14. https://doi.org/10.14814/phy2.13090

Rombough, P. J. (1999). The gill of fish larvae. Is it primarily a respiratory or an ionoregulatory structure? *Journal of Fish Biology*, *55*(SUPPL. A), 186–204.

https://doi.org/10.1006/jfbi.1999.1063

Segner, H., Storch, V., Reinecke, M., & Kloas, W. (1994). The development of functional digestive and metabolic organs in turbot, Scophthalmus maximus. *Marine Biology*, *119*(3), 471–486. https://doi.org/10.1007/BF00347544

Smith, T. I. J., Denson, M. R., Heyward, L. D., Jenkins, W. E., & Carter, L. M. (1999). Salinity effects on early life stages of southern flounder (Paralichthys lethostigma). *Journal of the World Aquaculture Society*, *30*(2), 236–244. https://doi.org/10.1111/j.1749-7345.1999.tb00870.x

Stiffler, D. F., Graham, J. B., Dickson, K. A., & Stockmann, W. (1986). Cutaneous Ion Transport in the Freshwater Teleost Synbranchus marmoratus. *Physiological Zoology*, 59(4), 406-418.

Tandler, A., Anav, F. A., & Choshniak, I. (1995). The effect of salinity on growth rate, survival and swimbladder inflation in gilthead seabream, Sparus aurata, larvae. *Aquaculture*, *135*(4), 343–353. https://doi.org/10.1016/0044-8486(95)01029-7

Thomas, J. C. (1968). Fish Bulletin 142. Management of The White Seabass (Cynoscion nobilis) in California Waters. Retrieved from https://escholarship.org/uc/item/3t10h9kr

Varsamos, S., Diaz, J. P., Charmantier, G. U. Y., Flik, G., Blasco, C., & Connes, R. (2002). Branchial chloride cells in sea bass (Dicentrarchus labrax) adapted to fresh water, seawater, and doubly concentrated seawater. *Journal of Experimental Zoology*, *293*(1), 12–26. https://doi.org/10.1002/jez.10099

Varsamos, S., Nebel, C., & Charmantier, G. (2005). Ontogeny of osmoregulation in postembryonic fish: A review. *Comparative Biochemistry and Physiology - A Molecular and Integrative Physiology*, *141*(4 SPEC. ISS.), 401–429. https://doi.org/10.1016/j.cbpb.2005.01.013

Vojkovich, M., & Reed, R. J. (1983). White Seabass, Atractoscion nobilis, in California-Mexican waters: tatus of the fishery. *California Cooperative Oceanic Fisheries Investigations Reports*, *XXIV*(Figure 2), 79–83.

Watanabe, S., Kaneko, T., & Watanabe, Y. (1999). Immunocytochemical detection of mitochondria-rich cells in the brood pouch epithelium of the pipefish, Syngnathus schlegeli: Structural comparison with mitochondria-rich cells in the gills and larval epidermis. *Cell and Tissue Research*, *295*(1), 141–149. https://doi.org/10.1007/s004410051220

White Seabass. *California Department of Fish and Wildlife*. Retrieved from https://www.wildlife.ca.gov/Conservation/Marine/NCCFRMP/White-Seabass

Weiner, S. (2003). An Overview of Biomineralization Processes and the Problem of the Vital Effect. *Reviews in Mineralogy and Geochemistry*, *54*(1), 1–29. https://doi.org/10.2113/0540001

Wexler, J. B., Margulies, D., & Scholey, V. P. (2011). Temperature and dissolved oxygen requirements for survival of yellowfin tuna, Thunnus albacares, larvae. *Journal of Experimental Marine Biology and Ecology*, *404*(1–2), 63–72. https://doi.org/10.1016/j.jembe.2011.05.002

Wu, S.-C., Horng, J.-L., Liu, S.-T., Hwang, P.-P., Wen, Z.-H., Lin, C.-S., & Lin, L.-Y. (2010). Ammonium-dependent sodium uptake in mitochondrion-rich cells of medaka (Oryzias latipes) larvae. *American Journal of Physiology-Cell Physiology*, *298*(2), C237–C250. https://doi.org/10.1152/ajpcell.00373.2009

Zydlewski, J. & McCormick, S.D. (2001). Developmental and environmental regulation of chloride cells in young American shad, Alosa sapidissima. *Journal of Experimental Zoology*, *290*(2), 73–87. https://doi.org/10.1002/jez.1037